Iron isotope fractionation in soil and graminaceous crops after 100 years of liming in the long-term agricultural experimental site at Berlin-Dahlem, Germany

Running title: Fe isotope fractionation in Luvisol and winter rye

B. WU[a,*], Y. WANG[a], A. E. BERNS[a], K. SCHWEITZER[c], S. L. BAUKE[b], R. BOL[a] & W. AMELUNG[a,b]

[a] *Institute of Bio- and Geosciences: Agrosphere (IBG-3), Forschungszentrum Jülich, Wilhelm-Johnen-Straße, 52428 Jülich, Germany*

[b] *Institute of Crop Science and Resource Conservation, Soil Science and Soil Ecology, University of Bonn, Nussallee 13, 53115 Bonn, Germany*

[c] *Department of Crop and Animal Sciences, Humboldt-Universität zu Berlin, Unter den Linden 6, 10099 Berlin, Germany*

* Correspondence: B. Wu. E-mail: b.wu@fz-juelich.de

Abstract

Sustainable arable cropping relies on repeated liming. Yet, the associated increase in soil pH can reduce the availability of iron (Fe) to plants. We hypothesized that repeated liming, but not pedogenic processes such as lessivage (i.e., translocation of clay particles), alters the Fe cycle in Luvisol soil, therewith affecting Fe isotope composition in soils and crops. Hence, we analyzed Fe concentrations and isotope compositions in soil profiles and winter rye from the long-term agricultural experimental site in Berlin-Dahlem, Germany, where a controlled liming trial with three field replicates per treatment has been conducted on Albic Luvisols since 1923. Heterogeneity in subsoil was observed at this site for Fe concentration but not for Fe isotope composition. Lessivage had not affected Fe isotope composition in the soil profiles. The results also showed that almost 100 years of liming lowered the concentration of the HCl-extractable Fe that was potentially available for plant uptake in the surface soil (0-15 cm) from 1.03 (SE 0.03) to 0.94 (SE 0.01) g kg^{-1}. This HCl-extractable Fe pool contained isotopically lighter Fe ($\delta^{56}Fe$ = -0.05 to -0.29‰) than the bulk soil ($\delta^{56}Fe$ = -0.08 to 0.08‰). However, its Fe isotope composition was not altered by the long-term lime application. Liming resulted in relatively lower Fe concentrations in the roots of winter rye. In addition, liming led to a heavier Fe isotope composition of the whole plants compared with those grown in the non-limed plots ($\delta^{56}Fe_{WholePlant\_+Lime}$ = -0.12‰ SE 0.03 vs. $\delta^{56}Fe_{WholePlant\_-Lime}$ = -0.21‰ SE 0.01). This suggests that the elevated soil pH (increased by 1 unit due to liming) promoted the Fe uptake strategy through complexation of Fe(III) from the rhizosphere, which favoured heavier Fe isotopes. Overall, the present study showed that liming and related increase in pH did not affect the Fe isotope compositions of the soil, but may influence the Fe

isotope composition of plants grown in the soil if they alter their Fe uptake strategy upon the change of Fe availability.

Highlights

- Fe concentrations and stocks, but not Fe isotope compositions, were more heterogeneous in subsoil than in topsoil
- Translocation of clay minerals did not result in Fe isotope fractionation in soil profile of Luvisol
- Liming decreased Fe availability in topsoil, but did not affect its $\delta^{56}Fe$ values
- Uptake of heavier Fe isotopes by graminaceous crops was more pronounced at elevated pH

Keywords

$\delta^{56}Fe$, plant-available Fe pool in soil, liming, winter rye

1. Introduction

As an essential nutrient, iron (Fe) is involved in numerous physiological processes, such as respiration, photosynthesis and DNA biosynthesis (Marschner, 1995; Kappler & Straub, 2005; Weber *et al*., 2006). Bioavailable Fe(II) is rapidly oxidized to Fe(III) in the presence of oxygen and subsequently forms Fe(III) (hydr)oxides, the solubility of which drastically decreases with increasing pH (Blume *et al*., 2016). Particularly in calcareous soils, severe Fe deficiency in plants may occur due to poor Fe availability under these pH conditions (Chen & Barak, 1982). In agricultural production systems, Fe availability may be reduced due to liming that is needed to maintain soil structure, to balance soil acidity, to optimize the supply of other essential nutrients like P, and to replenish base metal nutrients (i.e., calcium (Ca) and magnesium (Mg)) (Bolan *et al*., 2003; Haynes & Naidu, 1998). Over-application of lime may cause plants to take up Fe in a non-physiological form, leading to Fe deficiency in plants (lime-induced chlorosis) (e.g., Fageria *et al.*, 1995; Blume *et al.*, 2016).

Plants acquire Fe from the rhizosphere either through reduction or complexation strategies, so-called strategy I and II, respectively. Uptake strategy II is mainly used by graminaceous plants, including important staple crops such as rice, wheat and barley, by secreting phytosiderophores from their roots and forming Fe(III)-phytosiderophore complexes to improve Fe solubility in the rhizosphere (Mori, 1999; Shojima *et al*., 1990). However, Fe use by plants may not be restricted to one uptake strategy. Recent studies indicate that strategy I plants can also secrete Fe-binding compounds (e.g. Fourcroy *et al*., 2014; Rodriguez-Celma *et al*., 2018), while functional Fe(II) transporters have also been found in rice (Ishimaru *et al*., 2006). In any case, both Fe uptake into, and

translocation and transformation within, plants can result in Fe isotope fractionation, the extent of which can be different in graminaceous and non-graminaceous plants (e.g., Kiczka *et al*., 2010; Guelke-Stelling & von Blanckenburg, 2012). Non-graminaceous plants, utilizing the reduction strategy, tend to take up lighter Fe isotopes that are preferentially released during reductive dissolution of Fe-containing minerals in soil (Wiederhold *et al*., 2006; see also Wu *et al*., 2019 for a review). Kiczka *et al*. (2010) illustrated how Fe isotope fractionation might take place in non-graminaceous plants. However, mechanisms of Fe isotope fractionation in graminaceous plants still remain unclear owing to inconsistent fractionation effects described among the limited number of studies (Wu *et al.*, 2019, see also Figure SI1). Kiczka *et al.* (2010) and Guelke-Stelling and von Blankenburg (2012) argued that the Fe isotopic signature of a plant did not only depend on the Fe uptake strategy, but also on the nutrient availability in the growth substrate. This statement was only recently confirmed by a study where rice plants showed different Fe isotope compositions when growing under Fe-sufficient or Fe-deficient conditions (Liu *et al*., 2019). However, evidence of varying Fe isotope compositions upon different Fe availabilities is still needed to better understand Fe isotope fractionation in other graminaceous plants.

In the present study, we sampled soils and graminaceous crops (winter rye) at the long-term agricultural experimental site in Berlin-Dahlem, Germany, which had received liming treatments for almost 100 years (Krzysch *et al*., 1992). The soil at the studied site was an Albic Luvisol, for which we analyzed Fe isotope compositions of the soil profiles down to the depth of 100 cm to test the hypothesis (I) that physical clay illuviation during pedogenesis has not altered Fe isotope composition in the soil. In addition, we studied

the HCl-extractable Fe pool to test the hypothesis (II) that long-term liming practices would affect Fe pools that are potentially available for plant uptake. Finally, we analyzed Fe concentrations and isotope compositions of the winter rye plants grown in limed and non-limed plots to test the hypothesis (III) that Fe uptake by the crop plants would be altered due to changed soil conditions after liming, which would eventually be reflected by Fe isotope signatures of the crop grown in the limed soil.

2. Materials and methods

2.1 Site, sampling and sample pre-treatment

The soils and plants were sampled at the long-term Static Soil Use Experiment (BDa_D3) in Berlin-Dahlem, Germany (52°28'02"N 13°17'49"E) (Figure S2, detailed site decription can be found in the Supporting Information section, and in Krzysch *et al.*, 1992). The soils were characterized as Albic Luvisols according to the World Reference Base (IUSS Working Group WRB, 2015). Liming practice has been performed since 1923 to study its effect on soil and crop performance (Krzysch *et al.*, 1992). Dolomitic lime was applied in spring 2014 and 2016 at a rate of 250 kg CaO ha^{-1} a^{-1}. In the limed plots (+L1, +L2 and +L3) the soil pH was generally about 1 unit higher than in the three plots without lime application (-L1, -L2 and -L3) (Figure S3). The crop at the sampling time was winter rye (*Secale cereale* L.).

The soil sampling took place in April 2016 before renewed liming. Two soil cores were taken at diagonally opposing corners of each plots s down to 100 cm depth with a soil auger of 6-cm inner diameter, which was lined with an inner plastic sleeve for sample recovery (Walter *et al.*, 2016). The soil cores were divided into six segments, representing

the depths of 0-15, 15-30, 30-40, 40-50, 50-70 and 70-100 cm, respectively. The corresponding soil core segments of the two cores taken in one plot were well mixed on site and sub-sampled for the present study. In each plot, at least 10 winter rye plants were sampled at flowering stage in May 2017 and separated into roots, stems, leaves and spikes. In total there were 18 soil samples (i.e. 6 soil segments × 3 field replicates) and 12 plant samples (4 organs × 3 field replicates) for each treatment (i.e. lime or no lime).

2.2 Sample preparation Total concentrations of Fe (Fe_{Total}) and other major elements in soil were analyzed after digestion of 0.05 g soil with 0.25 g lithium meta/tetraborate at 1050^{o}C for 3 h. For the purpose of Fe isotope study, pressurized microwave-assisted digestion (turboWAVE, Milestone Srl, Italy) was applied to digest soils in a mixture of concentrated HNO_3 and H_2O_2, which released about 80% to 100% of total Fe (Figure S4), termed as bulk Fe (Fe_{Bulk}). The Fe pool in the soil potentially available to plants was extracted by 0.5 M HCl for 24 hours (Fe_{HCl}), as this method did not induce Fe isotope fractionation during extraction (Wiederhold *et al.* 2007, Guelke *et al.*, 2012). Kiczka *et al.* (2011) showed that HCl might also dissolve Fe in silicate minerals that was not readily available to plants. In this regard, we termed this pool as “HCl-extractable Fe” instead of “plant-available Fe pool” in the following sections. Iron in winter rye organs was also extracted by the pressurized microwave-assisted digestion.

2.3 Iron purification and isotope analysis

Separation of Fe from matrix elements in the sample was performed in a customer-designed laminar flow box in a cleanroom at the Agrosphere Institute at

Forschungszentrum Jülich GmbH, using anion exchange chromatography resin (Bio-Rad AG1-X4, 200-400 mesh) following the published method of Dauphas *et al*., 2004. Iron isotope analysis was performed on multi-collector ICP-MS (MC-ICP-MS, Nu Plasma II, Nu Instruments Ltd., UK) coupled with a desolvating nebulizer system (Aridus II, Teledyne Cetac, USA) in high mass resolution mode with a mass resolving power ($Rp_{5,95\%}$) of >8000 at ion beam transmission of 10%. To correct instrumental mass bias, a strategy of standard-sample-standard bracketing was applied using IRMM-524a with a matched Fe concentration (500 ppb) to the samples.

2.4 Data calculation and statistics

The results of Fe isotope analysis in samples were expressed using IRMM-014 as the standard (recommended by Dauphas *et al*., 2017) as follows:

$$\delta^{56}Fe(‰) = \left(\frac{\frac{^{56}Fe_{sample}}{^{54}Fe_{sample}}}{\frac{^{56}Fe_{IRMM-014}}{^{54}Fe_{IRMM-014}}} - 1 \right) * 1000$$

Long-term external precision was achieved at 0.08‰ and 0.12‰ for $\delta^{56}Fe$ and $\delta^{57}Fe$, respectively, based on two times the standard deviation (SD) of the $\delta^{56}Fe$ values of the repeated measurement of the IRMM-524a during the analytical sessions. The three-isotope-plot (Figure S5) indicated the absence of mass-independent fractionation during the analyses. The analyses were validated by repeated and in-lab cross-checked measurements of the in-house standard for soil (Luvisol, collected at Klein-Altendorf Experimental Station (50°37'9'' N, 6°59'29'' E) of the University of Bonn, Germany) and the NIST SRM 1575a (Table S1).

Statistical analyses were performed using OriginPro (V. b9.2.272; OriginLab, 2015). The significance of differences in Fe concentration and isotope composition between samples from limed and non-limed plots (n=3 for each treatment) was assessed by performing two-sample t-test following an F-test for testing equality of variances, while the differences between topsoil and subsoil, among plant organs, or between plants and the HCl-extractable Fe pool of respective treatment (n=3 for each variant) were evaluated by paired-sample t-test. Significance of differences was accepted at $p < 0.05$. If a significant difference occurred, we performed the least-significant-difference (LSD) procedure. Detailed Materials and Methods can be found in the Supporting Information section.

3. Results

3.1 Iron concentration, stock and isotope composition in bulk soil

Total Fe concentration in the topsoil (0-30 cm) of both limed and non-limed plots were found to be similar and showed little spatial variation (Figures 1a, S6a). In contrast, Fe concentrations in subsoil varied among plots, especially in the soil core segments between the ploughing depth and 70 cm with a large range from about 5 to 20 g kg^{-1} (Figure S6a), reflecting heterogeneous material deposition during the last ice age (Chmielewski & Köhn, 1999). Only two plots (+L2 and +L3) were alike in their Fe concentrations at every depth. The smallest Fe concentrations below 40 cm were found in plot -L2, where the subsoil contained more silt and less clay than in the other plots (Hobley & Prater, 2019). Correspondingly, total Fe stocks varied in the subsoil with the

mean values of 1.86×10^5 (SE 0.33×10^5) and 1.76×10^5 (SE 0.38×10^5) kg ha^{-1} for limed and non-limed plots (Figure 2), respectively, without significant difference between the two treatments.

The Fe isotope compositions within the soil profiles down to 100 cm ($\delta^{56}Fe_{Profile}$) were 0.00‰ (SE 0.03) and 0.00‰ (SE 0.01) for the bulk soil of the limed and non-limed plots, respectively (Figure 1b), identical within error between the treatments and to the representative parent material (+0.01‰, 2SD 0.05, analytical error, n = 4, see SI for parent material collection). The lateral difference in $\delta^{56}Fe$ values within the same soil segment across the fields (≤ 0.16‰) was comparable to the vertical difference within a soil profile (≤ 0.13‰) (Table S2, Figure S7a).

3.2 HCl-extractable Fe pool in soil

The extraction by diluted HCl (Fe_{HCl}) targets the so-called plant-available Fe pool (Guelke *et al*., 2010), which includes water-soluble Fe, exchangeable Fe, organically sorbed/bound Fe and short-range-ordered Fe minerals (Wiederhold *et al*., 2007). Our soil profiles contained 10-19% of total Fe (Fe_{Total}) in the form of HCl-extractable Fe (Fe_{HCl}) (Figure S6b,c). The topsoil contained larger Fe_{HCl} fractions relative to the Fe_{Total} pool compared with the subsoil. Similar to the bulk soil, the Fe concentrations in the Fe_{HCl} pool were relatively homogeneous in the topsoil and heterogeneous in the subsoil (Figures 3a, S6b). The Fe_{HCl} concentration in the surface soil (0-15 cm) treated with lime was significantly less than in the non-limed treatment (LSD = 0.070 < difference of the means 0.092). In addition, greater Fe_{HCl} stocks in the soil down to 100 cm (Figure 2) were found

in the limed plots, although the difference between the limed and non-limed plots was not statistically significant ($p = 0.16$).

The Fe_{HCl} pool was isotopically lighter than Fe in bulk soil (Figures 3b, S7). The differences in $\delta^{56}Fe$ values between the Fe_{HCl} pool and the bulk soil, expressed as $\Delta^{56}Fe_{HCl\text{-}Bulk}$, ranged from -0.04 to -0.39‰ (Table S2). Unlike the limited isotope fractionation of the bulk soil profiles, the Fe isotope compositions of the Fe_{HCl} pool ($\delta^{56}Fe_{HCl}$) showed a decreasing pattern from -0.09‰ (SE of the mean of all six plots 0.01) in the topsoil (0-30 cm) to -0.23‰ (SE of the mean of all six plots 0.02) at 100 cm depth. The highest $\delta^{56}Fe_{HCl}$ values appeared in the soil core segment of 15-30 cm for both limed and non-limed fields. The Fe isotope compositions of the Fe_{HCl} pool did not vary significantly in limed and non-limed plots.

3.3 Iron concentration and isotope composition in winter rye

The Fe concentrations of winter rye roots tended to be less when grown in the limed plots than those in the non-limed plots (Figure 3a, S7), although the differences were not statistically significant across the field replicates ($p = 0.10$). Compared with the Fe_{HCl} pool in the topsoil (0-30 cm), the variations of Fe concentrations in the plant roots were considerably larger (coefficient of variation 0.14 vs. 0.03 and 0.30 vs. 0.06 for limed and non-limed treatments, respectively). Aboveground organs contained much smaller Fe concentrations than the roots, with the stems containing the least Fe per kg dry mass (Figure 3a).

In spite of the large variations of the Fe concentrations, the Fe isotope compositions in the roots were within a narrow range and did not differ between the plants grown in the

soils with or without lime application (-0.02‰, SE 0.03 vs. -0.04‰, SE 0.02; Figures 3b, S8, Table S3). In contrast, aboveground organs exhibited variable Fe isotope compositions ranging from -0.30 to -0.83‰, which was much lighter than those in the roots. Compared with the Fe_{HCl} pool of the topsoil where the roots were mainly located, the roots of winter rye presented similar or slightly heavier Fe isotope compositions with $\Delta^{56}Fe_{Root\text{-}HCl}$ values of 0.06 (SE 0.04) and 0.05 (SE 0.03) for limed and non-limed plots, respectively. It is noteworthy that the aboveground organs of winter rye, especially the leaves and the spikes, were enriched in relatively heavier Fe isotopes when grown in limed soil than those taken from the control plots without lime (Figure 3b), though the differences were not statistically significant ($p = 0.16$ for leaves and $p = 0.07$ for spikes).

4. Discussion

4.1 Total Fe and HCl-extractable Fe pools in the studied Luvisol

Previous studies showed that pedogenic processes can fractionate Fe isotopes in soil relative to the parent material, with resulting changes in $\delta^{56}Fe$ values from -0.52 to +0.72‰ in the studied soil profiles to date (Wu *et al.*, 2019). Under reducing conditions (e.g., Gleysols) dissolution of primary Fe-minerals preferentially releases isotopically light Fe(II) into solution, leaving a weathered residue enriched in heavy Fe isotopes, while the light Fe isotopes are translocated within the soil profile or exported laterally. However, under permanent oxidizing conditions or moderate soil weathering (e.g., Cambisols) Fe isotope fractionation can be limited throughout the soil profile. In addition, eluviation and illuviation processes can result in Fe-depleted and Fe-enriched zones with significant differences in Fe isotope compositions (e.g., Podzols). Albic Luvisols as studied here are characterized

by significant lessivage, i.e., the downward migration of clay particles in the field. However, this process did not induce significant Fe isotope fractionation, as each of the studied profiles showed relatively homogeneous Fe isotope compositions within the soil profiles with vertical variations of δ^{56}Fe values ≤ 0.13‰. The lack of Fe isotope fractionation clearly supported the theory of lessivage, indicating a physical mobilization of colloids, for instance, after snowmelt, or a simple physicochemical release of colloids at low ionic strength after moderate acidification (e.g., Rousseau *et al.*, 2004; Ryan & Gschwend, 1998). Our results demonstrated that the processes occurring in these soils did not necessarily involve significant chemical alteration of Fe pools, in contrast to those observed, e.g., during redox processes or podzolization in soils (Wu *et al*., 2019).

The investigated Luvisol received low precipitation (annual precipitation of 562 mm) and no water logging was observed during sampling due to the sandy texture. Aerobic conditions thus prevailed in the soil. The lack of stagnant water prevented a profound reductive dissolution of Fe-containing minerals, which would preferentially mobilize light Fe isotopes (Crosby *et al*. 2005, 2007; Wiederhold *et al*., 2006; Wu *et al*., 2019). In combination with the limited vertical water transport due to low precipitation amounts, no significant Fe isotope fractionation was observed in the studied soil profiles. These relatively uniform Fe isotope compositions throughout the profiles were in line with other aerobic soils studied in temperate climate, such as Cambisols, e.g., in France, Geramny, Switzerland, and Canada, without pronounced redoximorphic features (Fekiacova *et al*., 2013; Wiederhold *et al*., 2007).

The Fe pool extracted by diluted HCl (Fe_{HCl}) was suggested to be potentially available to plant uptake (Guelke *et al*. 2010). The contribution of organically sorbed/bound Fe to

282 the Fe_{HCl} pool was low, as the soil was poor in organic matter (0.06-0.71%). In addition,
283 water-extractable Fe could also be neglected in such an aerobic soil with limited amounts
284 of drainage water. We, therefore, suspect that the Fe_{HCl} fraction consisted largely of short-
285 range-ordered Fe mineralsin our soil. The subsoil contained similar or larger
286 concentrations of HCl-extractable Fe, reflecting its release from overall larger total Fe
287 stocks compared with the topsoil. However, the utilization of subsoil Fe by plants depends
288 not only on its pool size, but largely also on its availability and accessibility to plants, which
289 is usually much lower than in the surface soil due to its higher bulk density, lower air
290 permeability, higher physical resistance for the root, and lower contents of organic matter
291 and microbial biomass, which all contribute to overall limitations in root growth and
292 nutrient uptake (Kautz *et al.*, 2013; Blume *et al.*, 2016).

293 In contrast to the bulk soil, the Fe_{HCl} pool was characterized by a light Fe isotope
294 signature, likely due to isotopically lighter Fe in short-range-ordered Fe mineralsformed
295 after preferential dissolution followed by immediate precipitation in the presence of
296 oxygen (see review by Wu *et al.*, 2019). The vertical profiles of the $\delta^{56}Fe$ values of the
297 Fe_{HCl} pool indicated a stronger depletion of heavy Fe isotopes in the deeper soil layers of
298 both limed and non-limed plots, along with increasing amounts of extracted short-range-
299 ordered Fe minerals. In addition, compared with the subsoil, the topsoil was much more
300 influenced by the plants. The harvest and removal of isotopically light aboveground
301 organs, as well as the accumulation of the roots with relatively heavier Fe isotope
302 composition in the topsoil, might also result in the topsoil becoming isotopically heavier
303 over years compared with the subsoil.

Long-term liming resulted in an increase of pH on average by one unit (Figure S3). This indicated that Fe speciation in the soil might vary, and thus Fe isotope composition of the soil might also change (Lotfi-Kalahroodi et al., 2019). However, neither the Fe isotope compositions of the total Fe pools nor those of the HCl-extracted Fe pools were significantly affected by liming (Figure 1, 3b). We attribute this to the larger unchanged Fe pools compared with those altered by pH.

4.2 Iron accumulation and isotope fractionation in winter rye

As a graminaceous crop, winter rye plants likely utilize the complexation strategy (i.e. strategy II) upon Fe deficiency in which phytosiderophores are released from the plant root to mobilize Fe(III) compounds by complexation of Fe(III) and formation of Fe(III)-phytosiderophores in order to acquire Fe from the rhizosphere (Marschner *et al*., 1986). In our field, Fe deficiency symptoms were not observed and the crops produced similar yields in both limed and non-limed plots in the year of sampling in the field (Figure S9). This indicates that Fe was not a limiting factor at our site, even after long-term liming practice. However, we observed that the roots of winter rye in one of the limed plots (+L3) contained only about half the concentration of Fe compared with the plants of other plots. This finding indicates that Fe availability was considerably different in plot +L3 from that in the other plots (Ågren & Weih, 2012), although Fe concentrations of the Fe_{HCl} pool were similar among the plough layers of the plots. In addition, the plants grown in the limed plots tended to be enriched in heavier Fe isotopes compared with their counterparts growing in the non-limed plots ($\delta^{56}Fe_{WholePlant}$ -0.12‰, SE 0.03 vs. -0.21‰, SE 0.01,

based on mass balance calculation, see SI), suggesting that elevated pH due to liming favoured the uptake of heavy Fe isotopes.

In this regard, Fe isotope composition of the plants relative to the growth media (here assumed to be the Fe_{HCl} pool) may provide some information about the dominant Fe uptake strategy that the plants have utilized. When strategy I is used reduction of Fe(III) to Fe(II) in the rhizosphere would result in isotopically light Fe(II) being taken into the plant, leading to an enrichment of light Fe isotopes in the root epidermis and inner root tissues (and eventually the whole plant). On the other hand, complexation induces less Fe isotope fractionation (e.g., equilibrium fractionation between inorganic aqueous Fe(III) and Fe(III)-siderophore ~0.6‰ in $\delta^{56}Fe$, Dideriksen *et al.*, 2008) than reduction (e.g., equilibrium fractionation between aqueous Fe(III) and Fe(II) ~3‰ in $\delta^{56}Fe$, Johnson *et al.*, 2002). The Fe isotope composition of the whole plant would then only marginally differ from that of the plant-available Fe in the growth substrate. Iron isotope fractionation due to the uptake through complexation of Fe(III) would then depend on the variation of isotope compositions between different Fe(III) species in the rhizosphere and in the root epidermis. This phenomenon of varied isotope fractionation effects was observed for rice (Liu *et al*., 2019) that can utilize both Fe(III) and Fe(II) from the rhizosphere (Ishimaru *et al*., 2006; Kobayashi and Nishizawa, 2012). At our site, the difference between the Fe isotope compositions of the whole plant and the Fe_{HCl} pool ($\Delta^{56}Fe_{WholePlant\text{-}HCl\_Topsoil}$) was only marginal. We, therefore, suggest that as typical for graminacous plants, strategy II was the dominant pathway of Fe uptake in winter rye growing in our field, even though no symptoms for Fe deficiency were observed. However, we could not fully rule out the contributions of uptake strategy I for Fe acquisition, as the extent of Fe isotope

fractionation by either of the two different strategies is still uncertain. Under liming conditions, where the soil pH increased by one unit (Figure S3), the reduction of Fe(III) becomes less effective due to the fact that the pH may be beyond the optimum of the ferric chelate reductase present in the root epidermis (Morrissey & Guerinot, 2009). In contrast, the transport of Fe(III)-phytosiderophores can still be efficient at elevated pH through the complexation strategy (Schaaf *et al.*, 2004). Therefore, winter rye might more likely utilize strategy II for Fe uptake at higher pH, leading to relatively heavier Fe isotope compositions of the plants than those growing without lime (Table S3). However, to be able to use the Fe isotope composition as a tracer to elucidate Fe uptake by plants, further studies are needed on how and to what extent Fe isotope fractionation takes place in plants under different nutrient conditions.

Aboveground organs of winter rye were enriched in light Fe isotopes with a $\Delta^{56}Fe_{Shoot\text{-}Root}$ value of -0.50‰ (SE 0.07 of samples from all the six plots). We attribute this difference to the variation of Fe speciation during in-plant translocation and redistribution. To reach the xylem from the root epidermis, Fe is symplasmically transported in the form of Fe(III)-deoxymugineic acid or other forms of Fe(III)-phytosiderophores (Nozoye et al., 2011). In the xylem, Fe(III)-citrate is present in both non-graminaceous and graminaceous plants, while in graminaceous plants, additional (and more) Fe(III)-phytosiderophores are predominant (Ariga et al., 2014). This indicates that from the root epidermis to the xylem of graminaceous plants, Fe can always be present in its ferric forms and reduction of Fe(III) to Fe(II) likely does not occur. Therefore, Fe isotope compositions of the tissues would vary mainly owing to the change of the binding ligands and their respective abundance in the tissue. Morgan et al. (2010) showed a strong positive correlation

between measured Fe isotope fractionation factors and the Fe-binding affinities of chelating ligands. In addition, Fe(III)-phytosiderophores have been shown to be about 1.5‰ in δ^{56}Fe heavier than Fe(III)-citrate (Moynier et al., 2013). This suggests that the xylem can exhibit a lighter Fe isotope composition than the root epidermis or the cortex, because the xylem can contain a mixture of Fe(III)-phytosiderophores and isotopically lighter Fe(III)-citrate, while the root epidermis accumulates isotopically heavier Fe(III)-phytosiderophores. Driven by transpiration and root pressure, Fe is transported upwards in the xylem to aboveground organs with the productive organs and younger leaves importing additional Fe from the phloem (Curie et al., 2009). Unlike in the xylem, Fe in the phloem is mainly chelated with nicotianamine and deoxymugineic acid (Kato et al., 2010; Nishiyama *et al.*, 2012). As nicotianamine has a higher affinity to Fe(III) but forms the more stable Fe(II)-nicotianamine complex, the phloem sap may consist of a mixture of Fe(II) and Fe(III) species with a variation of up to 3‰ in δ^{56}Fe between the two species (Moynier et al., 2013). Hence, the phloem sap may exhibit a lighter Fe isotope signature compared with the xylem sap. The isotopically light Fe pool in the phloem is further transported into younger leaves and flowers/seeds and then store in seeds in its Fe(III) forms (e.g., Briat, 1999; Ravet *et al.*, 2008; Vazzola *et al.*, 2007). Younger organs are usually found to be enriched in light Fe isotopes as suggested by Kiczka *et al.* (2010) and Guelke-Stelling & von Blanckenburg (2012). However, heavier Fe isotope compositions in seeds compared with other organs have also been observed (e.g., Arnold *et al.*, 2015; Moynier *et al.*, 2013, Figure S1). Our data showed that the Fe isotope compositions of the spikes of winter rye were similar to those of the leaves but lighter than the stems. The variable difference in Fe isotope signatures between seeds and straws among plant

species is likely because seeds receive Fe either via xylem vessels or via the sieve tubes of the phloem, as both circulate around the seed coat (Grillet *et al.*, 2014). The contribution of each Fe pathway varies among plant species depending on the presence of xylem discontinuity at the base of seeds, especially those of cereal crops, as demonstrated for Zn by Stomph *et al.* (2009). In addition, we observed that, despite the fact that each analyzed plant sample was a pooled sample of several individual plants, the δ^{56}Fe values of the same plant aboveground organ from the same treatment still differed by up to 0.2‰ (in leaves and spikes). We could thus conclude that the variation of Fe isotope composition of individual plants can even be larger, as shown by Kiczka *et al*. (2010) and Moynier *et al*. (2013), reflecting a varying extent of Fe isotope fractionation during in-plant translocation and redistribution.

5. Conclusion

The present study confirmed our hypothesis that physical pedogenic processes such as clay translocation through lessivage did not induce significant Fe isotope fractionation in the studied Albic Luvisol profiles, because this process involves the transport of colloids rather than of dissolved Fe. Long-term liming did also not enforce Fe isotope fractionation processes in the soil, but it led to heavier Fe isotope compositions in winter rye, suggesting that the plants responded to liming by increased Fe uptake through complexation processes. Our finding indicates that the analysis of Fe isotope compositions of field-grown plants is a promising tool for tracing alternations in Fe uptake strategies by plants under changed environmental conditions.

Supporting Information

Materials and Methods in detail

Equations for **error propagation**

Discussion of the effect of varied extraction rates by non-HF microwave-assisted digestion on Fe isotope composition of the total Fe pool in soil

Figure S1 Iron isotope compositions of the organs of graminaceous plants, which use the complexation strategy (strategy II) for Fe uptake. The vertical lines/bars indicate the Fe isotope compositions of plant-available Fe in the growth media, except for those in Moynier et al (2013) indicating the $\delta^{56}Fe$ value of the bulk soil. The colors of the vertical lines/bars correspond to respective data dots. The stars indicate Fe isotope compositions of shoots including stems/straws and leaves which were analyzed as a whole. The black boxplots present to-date available Fe isotopic data for graminaceous plants. Top lane: this study; black: -Lime; red: +Lime.

Figure S2 Soil texture change (from sandy to loamy) in the studied filed

Figure S3 Soil pH values in the investigated plots

Figure S4 The ratio of Fe in bulk soil extracted by pressurized microwave-assisted digestion (Fe_{Bulk}) to that extracted by lithium meta/tetraborate digestion (Fe_{Total})

Figure S5 Three-isotope-plot displaying measured $\delta^{56}Fe$ and $\delta^{57}Fe$ values of Fe in bulk soil, the HCl-extracted Fe pool, and Fe in plant organs

Figure S6 Iron concentrations of the total Fe pool (Fe_{Total}) (a) and in the HCl-extractable Fe pool (Fe_{HCl}) (b), and the ratio of Fe_{HCl} to Fe_{Total} (c) in the studied soil profiles

Figure S7 Iron isotope compositions of the bulk soil (Fe_{Bulk}) and the Fe_{HCl} pools in each individual plot

Figure S8 Iron concentrations and Fe isotope compositions in various winter rye organs grown in the soils treated with and without lime.

Figure S9 Dry biomass of the straw and the grain of winter rye at the harvest in the experimental field in 2017

Figure S10 Estimated Fe isotope compositions of the total Fe pool in the investigated soil profiles

Table S1 Iron concentrations and δ^{56}Fe values of the in-house standard for soils and the NIST SRM 1575a

Table S2 Iron concentrations, stock, and isotope compositions of the total Fe pool and HCl-extractable Fe pool in the studied limed and non-limed plots

Table S3 Dry biomass, Fe concentrations and isotope compositions of the plant (winter rye) samples

Data Availability Statement

The data of current study will be available at BonaRes Data Portal: https://datenzentrum.bonares.de/research-data.php.

Conflict of Interest Statement

We state that this work has no conflict of interest.

Acknowledgments

This work was supported by the German Federal Ministry of Education and Research (BMBF) in the framework of the funding initiative “Soil as a Sustainable Resource for the

Bioeconomy – BonaRes", project "BonaRes (Module A): Sustainable Subsoil Management - Soil^3; subproject 3" [grant numbers 031B0026C, 2015]. Prof. Dr. Jan Vanderborght at the Agrosphere Institute at Forschungszentrum Jülich GmbH is acknowledged for the discussion of statistical analyses of the data. We thank the Editer-in-Chief of the European Journal of Soil Science Prof. Jennifer Dungait and the two anonymous reviewers for their constructional suggestions on this study.

References

Ariga, T., Hazama, K., Yanagisawa, S. & Yoneyama, T. (2014). Chemical forms of iron in xylem sap from graminaceous and non-graminaceous plants. Soil Science and Plant Nutrition, 60, 460-469. doi:10.1080/00380768.2014.922406

Ågren, G. I. & Weih, M. (2012). Plant stoichiometry at different scales: element concentration patterns reflect environment more than genotype. New Phytologst, 194, 944-952. doi:10.1111/j.1469-8137.2012.04114.x

Blume, H.-P., Brümmer, G. W., Fleige, H., Horn, R., Kandeler, E., Kögel-Knabner, I., Kretzschmar, R., Stahr, K. & Wilke, B.-M. (2016). Scheffer/Schachtschabel Soil Science (1st English ed.). Springer-Verlag, Berlin Heidelberg. ISBN: 978-3-642-30941-0 (PB), ISBN: 978-3-642-30942-7 (E-Book). doi:10.1007/978-3-642-30942-7

Bolan, N. S., Adriano, D. C. & Curtin, D. (2003). Soil acidification and liming interactions with nutrient and heavy metal transformation and bioavailability. Advances in Agronomy, 78, 215-272. doi:10.1016/S0065-2113(02)78006-1

Briat, J. F. (1999). Plant ferritin and human iron deficiency. Nature Biotechnology, 17, 621. doi: 10.1038/10797

Chen, Y. & Barak P. (1982). Iron nutrition of plants in calcareous Soils. Advances in Agronomy, 35, 217-240. doi:10.1016/S0065-2113(08)60326-0

Chmielewski, F.-M. & Köhn, W. (1999). The long-term agrometeorological field experiment at Berlin-Dahlem, Germany. Agricultural and Forest Meteorology, 96, 39-48. doi:10.1016/S0168-1923(99)00045-3

Crosby, H. A., Johnson, C. M., Roden, E. E. & Beard, B. L. (2005). Coupled Fe(II)-Fe(III) electron and atom exchange as a mechanism for Fe isotope fractionation during dissimilatory iron oxide reduction. Environmental Science & Technology, 39, 6698-6704. doi:10.1021/es0505346

Crosby, H. A., Roden, E. E., Johnson, C. M. & Beard, B. L. (2007). The mechanisms of iron isotope fractionation produced during dissimilatory Fe(III) reduction by Shewanella putrefaciens and Geobacter sulfurreducens. Geobiology, 5, 169–189. doi:10.1111/j.1472-4669.2007.00103.x

Curie, C., Cassin, G., Couch, D., Divol, F., Higuchi, K., Le Jean, M., Misson, J., Schikora, A., Czernic, P. & Mari, S. (2009). Metal movement within the plant: contribution of nicotianamine and YELLOW STRIPE1-LIKE transporters. Annals of Botany, 103, 1–11. doi:10.1093/aob/mcn207

Dauphas, N., Janney, P. E., Mendybaev, R. A., Wadhwa, M., Richter, F. M., Davis, A. M., van Zuilen, M., Hines, R. & Foley, C. N. (2004). Chromatographic separation and multicollection-ICPMS analysis of iron. Investigating mass-dependent and –independent isotope effects. Analytical Chemistry, 76, 5855-5863. doi:10.1021/ac0497095

509 Dauphas, N., John, S. & Rouxel, O. (2017). Iron isotope systematics. Reviews in
510 Mineralogy and Geochemistry, 82, 415-510. doi:10.2138/rmg.2017.82.11
511 Dideriksen, K., Baker, J. A. & Stipp S. L. S. (2008). Equilibrium Fe isotope fractionation
512 between inorganic aqueous Fe(III) and the siderophore complex, Fe(III)-
513 desferrioxamine B. Earth and Planetary Science Letters, 269, 280-290.
514 doi:10.1016/j.epsl.2008.02.022
515 Fageria, N. K., Zimmermann, F. J. P. & Baligar, V. C. (1995). Lime and phosphorus
516 interactions on growth and nutrient uptake by upland rice, wheat, common bean, and
517 corn in an oxisol. Journal of Plant Nutrition, 18, 2519-2532.
518 doi:10.1080/01904169509365081
519 Fekiacova, Z., Pichat, S., Cornu, S. & Balesdent, J. (2013). Inferences from the vertical
520 distribution of Fe isotopic compositions on pedogenetic processes in soils. Geoderma,
521 209–210, 110-118. doi:10.1016/j.geoderma.2013.06.007
522 Fourcroy, P., Sisó-Terraza, P., Sudre, D., Savirón, M., Reyt, G., Gaymard, F., Abadía, A.;
523 Abadia, J.; Álvarez-Fernández, A.; Briat, J.-F. (2014). Involvement of the ABCG37
524 transporter in secretion of scopoletin and derivatives by Arabidopsis roots in response
525 to iron deficiency. New Phytologist, 201, 155–167. doi:10.1111/nph.12471
526 Grillet, L., Mari, S. & Schmidt, W. (2014). Iron in seeds – loading pathways and subcellular
527 localization. Frontiers in Plant Science, 4, 535. doi:10.3389/fpls.2013.00535
528 Guelke, M., von Blanckenburg, F., Schoenberg, R., Staubwasser, M. & Stuetzel H. (2010).
529 Determining the stable Fe isotopic signature of plant-available iron in soils. Chemical
530 Geology, 277, 269–280. doi:10.1016/j.chemgeo.2010.08.010

Guelke-Stelling, M. & von Blanckenburg, F. (2012). Fe isotope fractionation caused by translocation of iron during growth of bean and oat as models of strategy I and II plants. Plant and Soil, 352, 217–231. doi:10.1007/s11104-011-0990-9

Haynes R. J. & Naidu, R. (1998). Influence of lime, fertilizer and manure applications on soil organic matter content and soil physical conditions: a review. Nutrient Cycling in Agroecosystems, 51, 123–137. doi:10.1023/A:1009738307837

Hobley, E. U. & Prater, I. (2019). Estimating soil texture from vis–NIR spectra. European Journal of Soil Science, 70, 83-95. doi:10.1111/ejss.12733

Ishimaru, Y., Suzuki, M., Tsukamoto, T., Suzuki, K., Nakazono, M., Kobayashi, T., Wada, Y., Watanabe, S., Matsuhashi, S., Takahashi, M., Nakanishi, H., Mori, S. & Nishizawa, N. K. (2006). Rice plants take up iron as an Fe^{3+}-phytosiderophore and as Fe^{2+}. The Plant Journal, 45, 335-346. doi:10.1111/j.1365-313X.2005.02624.x

IUSS Working Group WRB. (2015). World Reference Base for Soil Resources 2014, Update 2015, International Soil Classification System for Naming Soils. World Soil Resources Report 106. Food and Agriculture Organization of the United Nations, Rome.

Johnson, C. M., Skulan, J. L., Beard, B. L., Sun, H., Nealson, K. H. & Braterman, P. S. (2002). Isotopic fractionation between Fe(III) and Fe(II) in aqueous solutions. Earth and Planetary Science Letters, 195, 141-153. doi:10.1016/S0012-821X(01)00581-7

Kappler, A. & Straub, K. L. (2005). Geomicrobiological cycling of iron. Reviews in Mineralogy and Geochemistry, 59, 85-108. doi:10.2138/rmg.2005.59.5

Kato, M., Ishikawa, S., Inagaki, K., Chiba, K., Hayashi, H., Yanagisawa, S. & Yoneyama, T. (2010). Possible chemical forms of cadmium and varietal differences in cadmium

554 concentrations in the phloem sap of rice plants (*Oryza sativa L.*). Soil Science and
555 Plant Nutrition, 56, 839-847. DOI: 10.1111/j.1747-0765.2010.00514.x
556 Kautz, T., Amelung, W., Ewert, F., Gaiser, T., Horn, R., Jahn, R., Javaux, M., Kuzyakov,
557 Y., Munch, J.-C., Pätzold, S., Peth, S., Scherer, H. W., Schloter, M., Schneider, H.,
558 Vanderborght, J., Vetterlein, D., Wiesenberg, G. & Köpke, U. (2013). Nutrient
559 acquisition from the arable subsoil in temperateclimates: a review. Soil Biology and
560 Biochemistry, 57, 1003-1022. doi:10.1016/j.soilbio.2012.09.014
561 Kiczka, M., Wiederhold, J. G., Frommer, J., Voegelin, A., Kraemer, S. M., Bourdon, B. &
562 Kretzschmar R. (2011). Iron speciation and isotope fractionation during silicate
563 weathering and soil formation in an alpine glacier forefield chronosequence.
564 Geochimica et Cosmochimica Acta, 75, 5559-5573. doi:10.1016/j.gca.2011.07.008
565 Kiczka, M., Wiederhold, J. G., Kraemer, S. M., Bourdon, B. & Kretzschmar, R. (2010).
566 Iron isotope fractionation during plant uptake and translocation in alpine plants.
567 Environmental Science & Technology, 44, 6144–6150. doi:10.1021/es100863b
568 Krzysch, G., Gaesar, K., Becker, K., Brodowski, M., Dressler, U.-B., Grimm, J., Jancke,
569 G., Krause, S. & Schlenther, L. (1992). Einfluß von langjährig differenzierten
570 Bewirtschaftungsmaßnahmen und Umweltbelastungen auf Bodenfruchtbarkeit und
571 Ertragsleistung eines lehmigen Sandbodens (Influence of long-term differentiated
572 management measures and environmental pollution on soil fertility and yield of a
573 loamy sandy soil). Final Report of the Interdisciplinary Research Project, IFP 15/2, at
574 the Institute of Crop Research, Technische Universität Berlin. ISSN 0177-6673.
575 Lotfi-Kalahroodi, E., Pierson-Wickmann, A.-C., Guénet, H., Rouxel, O., Ponzevera, E.,
576 Bouhnik-LeCoz, M., Vantelon, D., Dia, A. & Davranche, M. (2019). Iron isotope

fractionation in iron-organic matter associations: Experimental evidence using filtration and ultrafiltration. Geochimica et Cosmochimica Acta, 250, 98-116. doi:10.1016/j.gca.2019.01.036

Liu, C., Gao, T., Liu, Y., Liu, J., Li, F., Chen, Z., Li, Y., Lv, Y., Song, Z., Reinfelder, J. R. & Huang W. (2019) Isotopic fingerprints indicate distinct strategies of Fe uptake in rice. Chemical Geology, 524, 323-328. doi:10.1016/j.chemgeo.2019.07.002

Marschner, H. (1995). Mineral Nutrition of Higher Plants. Academic Press, London. ISBN: 9780124735439 (PB), ISBN: 9780080571874 (Ebook)

Marschner, H., Römheld, V. & Kissel, M. (1986). Different strategies in higher plants in mobilization and uptake of iron. Journal of Plant Nutrition, 9, 695-713. doi:10.1080/01904168609363475

Morgan, J. L. L., Wasylenki, L. E., Nuester, J. & Anbar A. D. (2010). Fe isotope fractionation during equilibration of Fe−organic complexes. Environmental Science & Technology, 44, 6095–6101. doi:10.1021/es100906z

Mori, S. (1999). Iron acquisition by plants. Current Opinion in Plant Biology, 2, 250-253. doi:10.1016/S1369-5266(99)80043-0

Morrissey, J. & Guerinot, M. L. (2009). Iron uptake and transport in plants: The good, the bad, and the ionome. Chemical Reviews, 109, 4553–4567. doi:10.1021/cr900112r

Moynier, F., Fujii, T., Wang, K. & Foriel, J. (2013). Ab initio calculations of the Fe (II) and Fe (III) isotopic effects in citrates, nicotianamine, and phytosiderophore, and new Fe isotopic measurements in higher plants. Comptes Rendus Geoscience, 345, 230-240. doi:10.1016/j.crte.2013.05.003

599 Nishiyama, R., Kato, M., Nagata, S., Yanagisawa, S. & Yoneyama, T. (2012).
600 Identification of Zn-nicotianamine and Fe-2'-deoxymugineic acid in the phloem sap
601 from rice plants (*Oryza sativa L.*). Plant and Cell Physiology, 53, 381–390.
602 doi:10.1093/pcp/pcr188
603 OriginLab. (2015). OriginPro. Release b9.2.272., OriginLab, Northampton, MA.
604 Ravet, K., Touraine, B., Boucherez, J., Briat, J. F., Gaymard, F. & Cellier, F. (2008).
605 Ferritins control interaction between iron homeostasis and oxidative stress in
606 Arabidopsis. The Plant Journal, 57, 400-412. doi:10.1111/j.1365-313X.2008.03698.x.
607 Rodriguez-Celma, J., Green, R. T., Connorton, J. M., Kruse, I., Cui, Y., Ling, H. Q. & Balk,
608 J. (2018). BRUTUS-LIKE proteins moderate the transcriptional response to iron
609 deficiency in roots. bioRxiv (Preprint), doi:10.1101/231365
610 Ryan, J. N. & P. M. Gschwend. (1998). Effects of ionic strength and flow rate on colloid
611 release: relating kinetics to intersurface potential energy. Journal of Colloid and
612 Interface Science, 164, 21-34. doi:10.1006/jcis.1994.1139
613 Rousseau, M., Di Pietro, L., Angulo-Jaramillo, R., Teissier, D. & Cabidel, B. (2004).
614 Preferential transport of soil colloidal particles: physicochemical effects on particle
615 mobilization. Vadose Zone Journal, 3, 247. doi:10.2136/vzj2004.2470
616 Schaaf, G., Ludewig, U., Erenoglu, B. E,, Mori, S., Kitahara, T.& von Wirén, N. (2004).
617 ZmYS1 functions as a proton-coupled symporter for phytosiderophore- and
618 nicotianamine-chelated metals. Journal of Biological Chemistry, 279, 9091-9096.
619 doi:10.1074/jbc.M311799200

620 Shojima, S., Nishizawa, N.-K., Fushiya, S., Nozoe, S., Irifune, T. & Mori, S. (1990).
621 Biosynthesis of phytosiderophores. Plant Physiology, 93, 1497–1503.
622 doi:10.1104/pp.93.4.1497
623 Stomph, J. T., Jiang, W. & Struik, P.C. (2009). Zinc biofortification of cereals: rice differs
624 from wheat and barley. Trends in Plant Science, 14, 123-124.
625 doi:10.1016/j.tplants.2009.01.001.
626 Vazzola, V., Losa, A., Soave, C. & Murgia, I. (2007). Knockout of frataxin gene causes
627 embryo lethality in *Arabidopsis*. FEBS Letters, 581, 667-672.
628 doi:10.1016/j.febslet.2007.01.030
629 Walter, K., Don, A., Tiemeyer, B. & Freibauer, A. (2016). Determining soil bulk density for
630 carbon stock calculation: a systematic method comparison. Soil Science Society of
631 America Journal, 80, 579–591. doi:10.2136/sssaj2015.11.0407
632 Weber, K. A., Achenbach, L. A. & Coates, J. D. (2006). Microorganisms pumping iron:
633 anaerobic microbial iron oxidation and reduction. Nature, 4, 752-764.
634 doi:10.1038/nrmicro1490
635 Wiederhold, J. G., Kraemer, S. M., Teutsch, N., Borer, P. M., Halliday, A. N. &
636 Kretzschmar, R. (2006). Iron isotope fractionation during proton-promoted, ligand-
637 controlled, and reductive dissolution of goethite. Environmental Science & Technology,
638 40, 3787-3793. doi:10.1021/es052228y
639 Wiederhold, J. G., Teutsch, N., Kraemer, S. M., Halliday, A. N. & Kretzschmar, R. (2007).
640 Iron isotope fractionation in oxic soils by mineral weathering and podzolization.
641 Geochimica et Cosmochimica Acta, 71, 5821–5833. doi:10.1016/j.gca.2007.07.023

642 Wu, B., Amelung, W., Xing, Y., Bol, R. & Berns, A. E. (2019). Iron cycling and isotope
643 fractionation in terrestrial ecosystems. Earth-Science Reviews, 190, 323-352.
644 doi:10.1016/j.earscirev.2018.12.012
645

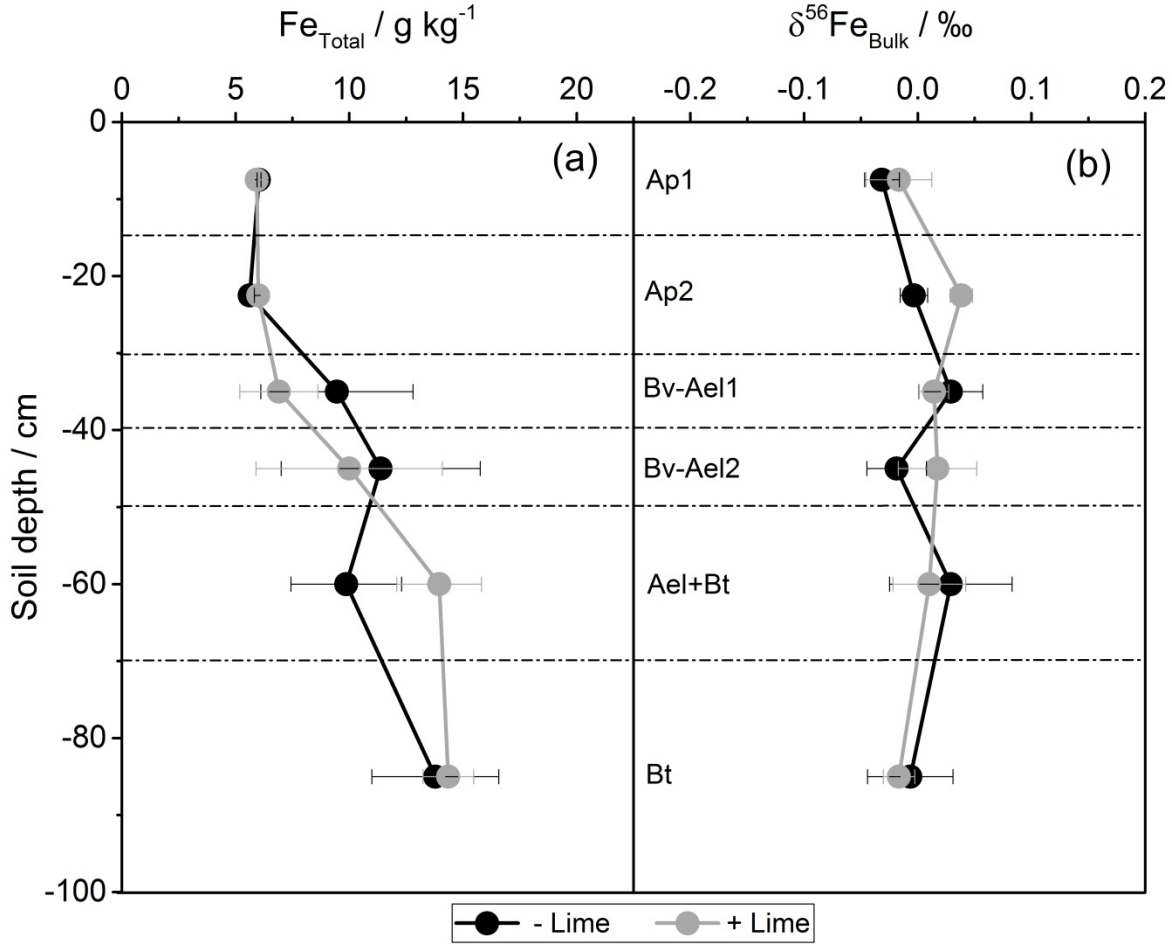

Figure 1 Depth profiles of total Fe concentrations (a) and isotope compositions (b) of the bulk soil at the long-term experimental field in Berlin-Dahlem. The horizontal dash lines indicate the analyzed soil core segments. The soil horizons are German descriptions of a representative key soil profile at the experimental site, where Ap is the ploughed topsoil, Bv-Ael and Ael correspond to an eluvial horizon, and Ael+Bt and Bt to an argic horizon according to World Reference Base (IUSS Working Group WRB, 2015). The bars are standard error of the mean of three field replicates for no-lime (black) and lime (gray) management, respectively, showing heterogeneity of subsoil, but not of the topsoil, with respect to Fe content. The studied Luvisol exhibited relatively uniform Fe isotope

compositions. Values between limed and non-limed plots were not statistically significant at the $p = 0.05$ level of probability.

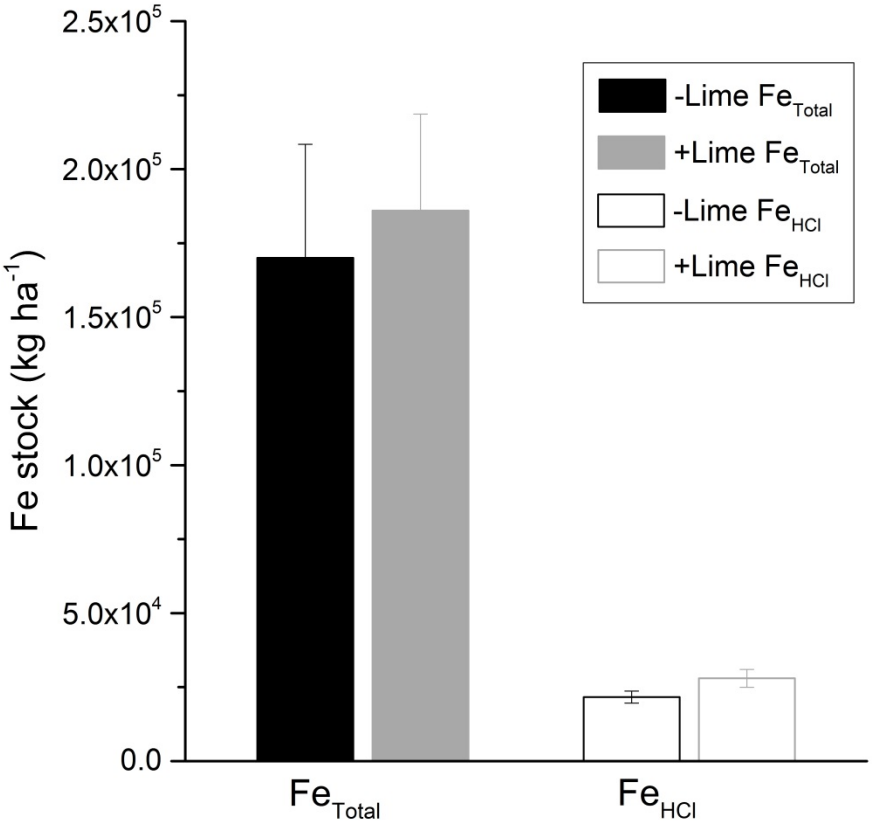

658

659 **Figure 2** Iron stocks of the total Fe pool (Fe_{Total}) and the plant-available Fe pool (Fe_{HCl})
660 in the limed (gray) and non-limed (black) plots within the soil depth of 0-100 cm. The bars
661 are standard error of the mean of three field replicates for no-lime (black) and lime (gray)
662 management, respectively. Values between limed and non-limed plots were not
663 statistically significant ($p = 0.05$).

664

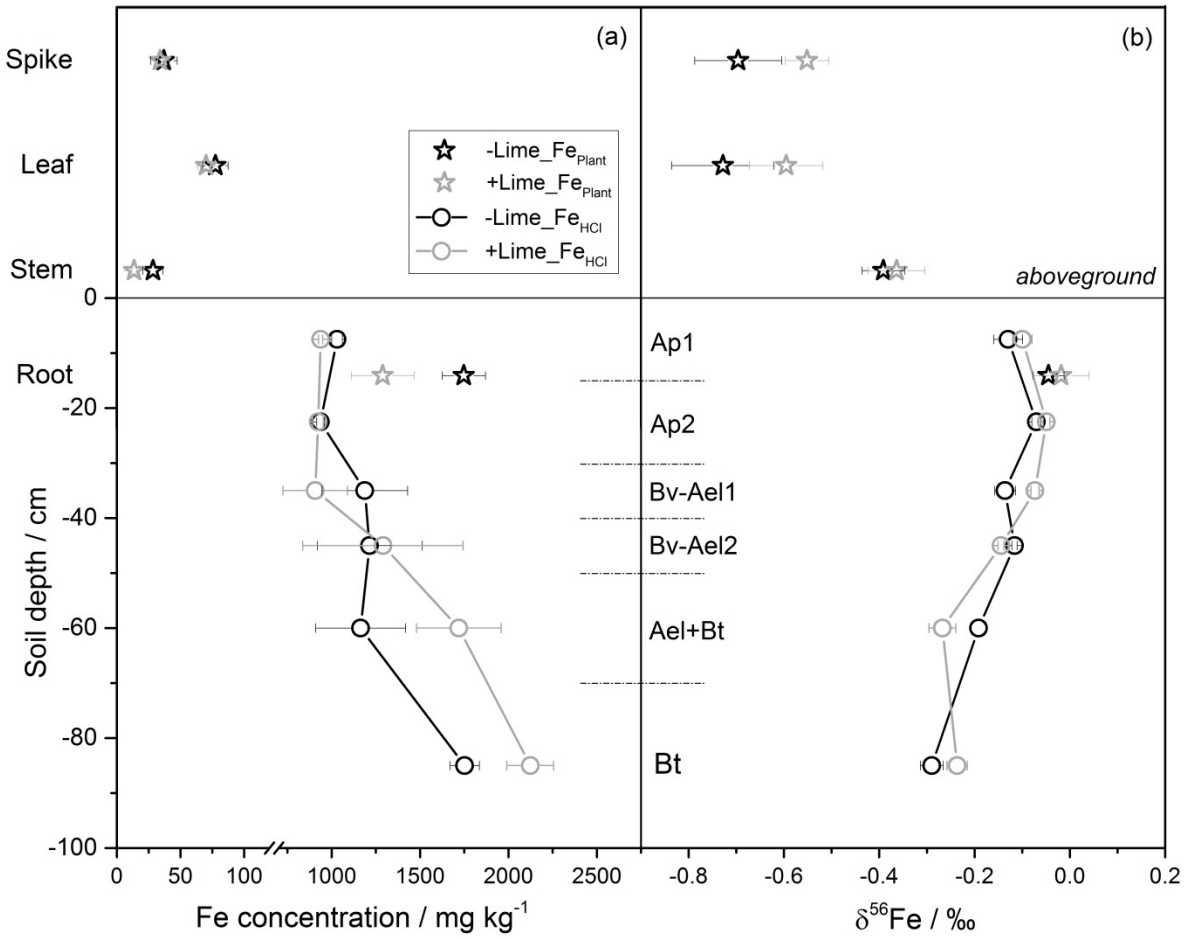

Figure 3 Iron concentrations (a) and isotope compositions (b) of the Fe_{HCl} pool representing the plant-available Fe in the soil core segments (circle) and of the organs of winter rye (Fe_{Plant}, star), showing that most Fe was accumulated in the roots of winter rye which exhibited the heaviest Fe isotope composition compared with either the aboveground organs or the Fe_{HCl} pool in the soil where they had grown. Winter rye plants grown in limed plots showed heavier Fe isotope compositions ($\delta^{56}Fe_{WholePlant\_+Lime}$ = -0.12‰ SE 0.03) than those grown in non-limed plots ($\delta^{56}Fe_{WholePlant\_-Lime}$ = -0.21‰ SE 0.01). Values between limed and non-limed plots were not statistically significant (p = 0.05), except for the Fe concentrations in the Fe_{HCl} pool in the soil layer 0-15 cm. The short

horizontal dash lines indicate the analyzed soil core segments. The soil horizons are German descriptions of a representative key soil profile at the experimental site, where Ap is the ploughed topsoil, Bv-Ael and Ael correspond to an eluvial horizon, and Ael+Bt and Bt to an argic horizon according to World Reference Base (IUSS Working Group WRB, 2015). The bars are standard error of the mean of three field replicates for no-lime (black) and lime (gray) management, respectively. Note that the plant tissues are not positioned on the true scale of their heights.

Iron isotope fractionation in soil and graminaceous crops after 100 years of liming in the long-term agricultural experimental site at Berlin-Dahlem, Germany

Running title: Fe isotope fractionation in Luvisol and winter rye

B. WU[a,*], Y. WANG[a], A. E. BERNS[a], K. SCHWEITZER[c], S. L. BAUKE[b], R. BOL[a] & W. AMELUNG[a,b]

[a] *Institute of Bio- and Geosciences: Agrosphere (IBG-3), Forschungszentrum Jülich, Wilhelm-Johnen-Straße, 52428 Jülich, Germany*

[b] *Soil Science and Soil Ecology, Institute of Crop Science and Resource Conservation, University of Bonn, Nussallee 13, 53115 Bonn, Germany*

[c] *Department of Crop and Animal Sciences, Humboldt-Universität zu Berlin, Unter den Linden 6, 10099 Berlin, Germany*

* Correspondence: B. Wu. E-mail: b.wu@fz-juelich.de

Supporting Information

Materials and Methods

Site, sampling and sample pre-treatment

The soil and plant were sampled at the long-term Static Soil Use Experiment (BDa_D3) in Berlin-Dahlem, Germany (52°28'02"N 13°17'49"E). The climate at the experimental site is classified as semi-continental with an average annual air temperature of 9.9°C and an annual precipitation of 562 mm (period 1981-2010) (Chmielewski & Köhn, 1999). The soils of the field are characterized as Albic Luvisols according to the World Reference Base (IUSS Working Group WRB, 2015) and were developed on quaternary deposits. The dominant parent material is periglacial sandy deposits overlying loam and glacial till. Generally, the topsoil (0-30 cm) contains 65-75% sand, 17-23% silt and 8-12% clay, while in the subsoil (30-100 cm) sand contents decrease to 40-60% and clay contents increase to 20-25% (Hobley & Prater, 2019). The subsoil is characterized by a high heterogeneity with regard to chemical and physical properties, which can be explained by the soil development during Weichselian Late Glacial (Chmielewski & Köhn, 1999). The depth of the texture changing from sandy and loamy varies from 40 to > 100 cm as previously shown by Sümer, 2012 (also see Supporting Information Figure S2). At depth lower than 60 cm calcareous glacial till can occur, resulting in pH values higher than 7. Soil organic matter contents are low with a range of 0.06-0.71%.

The BDa_D3 experiment was established in 1923 to investigate the impact of different soil management practices on soil properties, crop development and yield performances (Köhn & Ellmer, 2009). Five soil management factors are been investigated, each at two

levels: ploughing depth (deep, 28 cm / shallow, 17 cm), with / without liming, with / without phosphorous (P) fertilization, with / without farmyard manure application (FYM, since 1937), and crop rotation (leaf crop - cereal crop rotation / only cereal crops, period 1967-2013). Each treatment was performed in three field replicates. The actual crop rotation is maize (*Zea mays* L.) for silage – winter rye (*Secale cereale* L.).

In this study, the factor of liming was selected, each in combination with deep ploughed, with P (20 kg ha^{-1} a^{-1}) and FYM (30 t ha^{-1} in autumn 2013 and 2015) applications, and the leaf crop - cereal crop rotation. Dolomitic lime was applied in autumn 2013 and 2015 at a rate of 0.25 ton CaO ha^{-1} a^{-1} (long-term average 0.3 t CaO ha^{-1} a^{-1}). In the limed plots (+L1, +L2 and +L3) the soil pH was generally about 1 unit higher than the other three plots without lime application (-L1, -L2 and -L3) (Figure S3). The range of pH values from 5.0 to 7.6 ($CaCl_2$) at the limed plots indicates the conditions under which Fe availability in soil could be expected to be low (Sarkar & Wynjones 1982).

The soil sampling took place in April 2016. Two soil cores were taken at random places down to 100 cm depth from each plot with a soil auger of 6-cm inner diameter, which was lined with an inner plastic sleeve for sample recovery (Walter *et al*., 2016). The soil coring technique followed the outlines of the German Agricultural Soil Inventory, allowing a simultaneous assessment of bulk density (Walter *et al*., 2016). The technique was already successfully applied to other long-term agricultural research trials (Bauke *et al*., 2018; Hobley *et al*., 2018).

The soil cores were subdivided into sampling segments referring to a representative soil profile at the experimental site, which was confirmed by the soil coring in the experimental field. According to German soil classification system (Ad-hoc-AG Boden,

2005) the representative key soil profile was described as follows: Ap (0-30 cm depth), Bv-Ael (30-50 cm depth), Ael+Bt (50-70 cm depth) and Bt (70-100 cm depth). To avoid mixture of two different soil horizons in one sample, the soil core was divided into six segments, representing the horizons at the depths of 0-15, 15-30, 30-40, 40-50, 50-70 and 70-100 cm, respectively. The corresponding soil core segments of the two cores taken in one plot were well mixed on site and sub-sampled for the present study. A sample, considered to be representative of the parent materials, was collected from the C horizon below the developed soil at a location where soil development was the shallowest (site identified with the map shown in Sümer, 2012), from a subsite at which neither fertilization nor lime had been applied in the past. The soil samples were frozen at -20 ^{o}C before being lyophilized. After drying, the soils were gently ground in an agate mortar and then passed through 2-mm analytical sieve (Retsch, Germany). Dry bulk density and pH values of the soil samples were performed as described by Bauke *et al.* (2018) at University of Bonn.

Winter rye growing in the six investigated plots was collected at flowering stage in May 2017. In each plot, at least 10 individual plants were randomly chosen and carefully pulled out of the soil. After the attached soil had been shaken off, roots and aboveground organs were separated and immediately stored on site in cool boxes filled with dry ice. The aboveground plant organs were throughout washed with Milli-Q water and briefly dried with soft paper wipes. To remove soil particles adsorbed to the root surface, the roots were immerged in Milli-Q water and cleaned in an ultrasonic bath at room temperature for 10 min. The cleaned plant organs were then frozen at -20^{o}C before they were freeze-dried. The dried organs were weighted to document their dry biomass and then milled to

769 powder in a custom-designed ball mill (Collomix Viba 330, Collomix GmbH, Germany)
770 using metal-free plastic bottles and tungsten carbide milling balls. Both soil and plant
771 samples were stored under dry conditions before being further processed.
772
773 **Sample preparation**
774 Total concentrations of Fe (Fe_{Total}) and other major elements in soil were analyzed by
775 inductively coupled plasma optical emission spectrometry (ICP-OES, Thermo iCap,
776 Thermo Fischer Scientific, Germany) after digestion of 0.05 g soil with 0.25 g lithium
777 meta/tetraborate at 1050^{o}C for 3 h. Since lithium meta/tetraborate digestion introduces a
778 large amount of matrix to the samples, Fe isotope analyses were not performed for these
779 samples. Instead, pressurized microwave-assisted digestion (turboWAVE, Milestone Srl,
780 Italy) was applied to digest soils in a mixture of concentrated HNO_3 and H_2O_2 with the
781 purpose of Fe isotope composition analyses. Around 0.05 g soil was weighted into a PFA
782 microwave extraction tube and mixed with 3 ml distilled ultrapure HNO_3 (68%) and 1 ml
783 H_2O_2 (30%, p.a.). The soil-acid mixture then underwent a step-wised digestion program,
784 which released about 80% to 100% of total Fe (Figure S4), termed as bulk Fe (Fe_{Bulk}).
785 The remaining Fe in refractory compounds (e.g., in partial silicate minerals) was not
786 extracted, which would thus unlikely readily participate in the biogeochemical Fe cycle of
787 the soils. White/grayish sands were left after microwave-assisted digestion and discarded
788 after centrifugation at 5000 × g for 10 min. The supernatant was transferred into a round-
789 bottomed 15-ml PFA vial (Savillex, Eden Prairie, USA) and placed on a heating plate at
790 80 ^{o}C to be completely dried down. The dried materials were re-dissolved in 1 ml 6 M HCl
791 for further use. The Fe content in the re-dissolved sample was analyzed by inductively

coupled plasma mass spectrometry (ICP-MS, Agilent 7900, Agilent, Germany) and validated by comparing it with Fe content in the respective sample before drying down to ensure no Fe loss during the dry-down process.

To estimate the plant-available Fe pool in soil samples (Guelke *et al*., 2010), 1 g soil was weighed into a Falcon® centrifuge tube and added with 20 ml 0.5 M ultrapure HCl (Fe_{HCl}). The soil-HCl mixture was shaken for 24 h using a horizontal shaker at room temperature and centrifuged at 5000 × g for 15 min. The residue was washed twice with Milli-Q water and the wash solution was combined with the extracted supernatant after centrifugation. The extract was then filtered through a PTFE filter with a pore-size of 0.45 µm and transferred into a round-bottomed 22-ml Savillex PFA vial. After drying down at 80 °C, 0.5 ml ultrapure HNO_3 (68%) was added to the sample before carefully adding 0.5 ml H_2O_2 (30%, p.a.). The vials were firmly closed and heated at 80 °C for 30 min to fully oxidize the organic matters. The solution was then dried down again at 80 °C and re-dissolved in 1 ml 6 M ultrapure HCl for Fe purification. Iron content was monitored before and after each drying-down/re-dissolving process to ensure no Fe losses.

Fifty (roots) to one-hundred milligrams (aboveground) plant organs were weighted into the PFA microwave extraction tube and mixed with 5 ml distilled ultrapure HNO_3 (68%) and 2 ml H_2O_2 (30%, p.a.) for the microwave-assisted digestion. Due to the small amount of Fe present in the aboveground organs, digestions of two (leaves and spikes) to six (stems) samples were performed and combined for Fe isotope analysis of the respective organ. The microwave-assisted digestion could not fully digest the plant samples, since the silicates that had been accumulated in the rye were preserved. Each individual extract was centrifuged at 5000 × g for 10 min and the supernatant was dried down in a round-

bottomed 22-ml Savillex vial at 80 ºC. The dried materials were re-dissolved in 1 ml 6 M ultrapure HCl individually. The Fe content was analyzed by ICP-MS before and after the drying-down/re-dissolving process. Only when Fe in the extraction replicates was fully recovered (>95%) were the replicates mixed for Fe purification.

An in-house standard for soil (Luvisol, collected at Klein-Altendorf Experimental Station (50º37'9''N, 6º59'29''E) of the University of Bonn, Germany) and the NIST SRM 1575a were used as routine standards for the analyses of the soils and plants, respectively. In each individual microwave-assisted digestion sequence and the following procedures, either of these two standards was run together with the samples.

Iron purification and isotope analysis

The dry-down processes and Fe purification were carried out in customer-designed laminar flow box in a cleanroom at the Agrosphere Institute at Forschungszentrum Jülich GmbH. Iron purification was carried out using anion exchange chromatography resin (Bio-Rad AG1-X4, 200-400 mesh) following the published method of Dauphas *et al*., 2004. Aliquots of soil and root samples containing 10 µg Fe were loaded on 1 ml resin, while for aboveground organs the loaded Fe was usually less than 10 µg. The matrix elements were stepwise eluted by in total 10 ml 6 M ultrapure HCl (matrix cut) and then Fe was stepwise eluted by in total 6 ml 0.05 M ultrapure HCl (Fe cut). The Fe cut was then dried down at 80 ºC and re-dissolved in 1 ml 0.3 M ultrapure HNO_3 for Fe isotope analysis. For soil samples and plant roots and leaves, good recovery of Fe (>95%) and the absence of matrix elements was confirmed by analyzing Fe and other elements (e.g. Al, Si, Mg, Mn, Cu, Zn, etc.) in the Fe cut by ICP-MS. However, some Zn was detected in the Fe cut of

838 the plant stems and spikes, although a recovery of >95% was achieved for Fe. A
839 dissolved sample of Fe isotope standard IRMM-524a (original material of IRMM-014) and
840 an acid blank were analyzed in parallel with samples for quality control.

841 Iron isotope analysis was performed on multi-collector ICP-MS (MC-ICP-MS, Nu
842 Plasma II, Nu Instruments Ltd., UK) coupled with a desolvating nebulizer system (Aridus
843 II, Teledyne Cetac, USA), in high mass resolution mode with a mass resolving power
844 ($Rp_{5,95\%}$) of >8000 at ion beam transmission of 10%. To correct instrumental mass bias,
845 a strategy of standard-sample-standard bracketing was applied using IRMM-524a with a
846 matched Fe concentration (500 ppb) to the samples. For each of the samples containing
847 Zn, the Fe isotope standard was spiked with a Zn ICP-MS standard with the same Zn
848 concentration as in the sample and measured respectively with individual samples.
849 Although IRMM-524a was used during the measurement in the present study, the results
850 of Fe isotope analysis in samples were expressed using IRMM-014 as the standard
851 (recommended by Dauphas *et al*., 2017) as follows:

852 $$\delta^{56}Fe(‰) = \left(\frac{\frac{^{56}Fe_{sample}}{^{54}Fe_{sample}}}{\frac{^{56}Fe_{IRMM-014}}{^{54}Fe_{IRMM-014}}} - 1 \right) * 1000$$

853 Both δ^{56}Fe and δ^{57}Fe were analyzed to evaluate any possible mass-independent
854 isotope fractionation during the analysis. In addition, signals of ^{53}Cr were monitored in
855 order to correct any possible interference of ^{54}Cr on ^{54}Fe.

856 Long-term external precision was achieved at 0.08‰ and 0.12‰ for δ^{56}Fe and δ^{57}Fe,
857 respectively, based on two times the standard deviation (SD) of the δ^{56}Fe values of the
858 repeated measurement of the IRMM-524a during the analytical sessions. The three-

isotope-plot (Figure S5) indicated the absence of mass-independent fractionation during the analyses. The analyses were validated by repeated and in-lab cross-checked measurements of the in-house standard for soil and the NIST SRM 1575a (Table S1).

Data calculation and statistics

The Fe isotope compositions of aboveground shoot ($\delta^{56}Fe_{Shoot}$) and of the whole plant ($\delta^{56}Fe_{WholePlant}$) were calculated based on mass balance using:

$$\delta^{56}Fe_{Shoot\ or\ WholePlant} = \sum (\delta^{56}Fe_i \times \frac{m_i c_i}{\sum m_i c_i})$$

where m_i and c_i were the dry biomass and the Fe concentration of plant organ *i* (root, stem, leaf, or spike), respectively.

Similarly, the Fe isotope compositions of soil profiles of 0-100 cm ($\delta^{56}Fe_{Profile}$) or the entire experimental field ($\delta^{56}Fe_{Field}$) were calculated using:

$$\delta^{56}Fe_{Profile\ or\ Field} = \sum (\delta^{56}Fe_i \times \frac{D_i V_i c_i}{\sum D_i V_i c_i})$$

where D_i, V_i and c_i were the dry bulk density, the volume and the Fe concentration of the soil at the depth of soil core segment *i*, respectively

The apparent difference in Fe isotope composition in different Fe pools (i.e., Fe_{Bulk}, Fe_{HCl}, the plant organs and the whole plant) were calculated using:

$$\Delta^{56}Fe_{A-B} = \delta^{56}Fe_A - \delta^{56}Fe_B$$

The Fe concentrations, stocks, and isotope compositions of soil core segments and plant organs were given as the mean values of the three field replicates and the standard error (SE) of the mean, unless it was specifically stated.

Statistical analyses were performed using OriginPro (V. b9.2.272; OriginLab, 2015). The significance of differences in Fe concentration and isotope composition between samples from limed and non-limed plots was assessed by performing two-sample t-test following an F-test for testing equality of variances, while the differences between topsoil and subsoil, among plant organs, or between plants and the plant-available Fe pool with respective treatment were evaluated by paired-sample t-test. Significance of differences was accepted at $p < 0.05$. If a significant difference accrued, we performed the least-significant-difference procedure.

Error propagation

1. The 2SD of the calculated Fe isotope composition of the topsoil (0-30 cm) was computed as follows:

$$2SD_{Topsoil} = \sqrt{\sum_{i=0-15cm}^{15-30cm} (2SD_i \times \frac{Fe\ stock_i}{Fe\ stock_{Topsoil}})^2}$$

where *i* denoted soil layers of 0-15 cm and 15-30 cm.

A similar equation was applied to subsoil and the whole soil profile as well using respective SDs involved in the mass balance.

2. The 2SD of the calculated Fe isotope composition of the aboveground shoot or the whole plant was computed as follows:

$$2SD_{Shoot} = \sqrt{\sum_{i=Stem}^{Spike} (2SD_i \times \frac{m_i c_i}{\sum m_i c_i})^2}$$

$$2SD_{WholePlant} = \sqrt{\sum_{i=Root}^{Spike} (2SD_i \times \frac{m_i c_i}{\sum m_i c_i})^2}$$

where m_i and c_i were the dry biomass and the Fe concentration of plant organ *i* (root, stem, leaf, or spike), respectively.

A similar equation was applied to 2SD of the Fe isotope compositions of soil profiles of 0-100 cm or the entire experimental field.

3. The 2SD of the apparent variation of Fe isotope compositions between two Fe pools A and B was computed as follows:

$$2SD_{\Delta^{56}Fe_{A-B}} = \sqrt{(2SD_{\delta^{56}Fe_A})^2 + (2SD_{\delta^{56}Fe_B})^2}$$

Discussion of the effect of varied extraction rates by non-HF microwave-assisted digestion on Fe isotope composition of the total Fe pool in soil

It is noteworthy that Fe isotope compositions determined in this study were based on the bulk soil extracted by pressurized microwave-assisted digestion without HF which released variable amounts of Fe out of the total Fe depending on the mineralogical composition of the sample material (Schwartz & Kölbel, 1992). Our digestion method was more effective for samples with higher clay and lower sand contents. However, at elevated sand contents > 60%, only up to 20% of Fe could not be extracted by this non-HF microwave-assisted digestion (Figure S4). As HF is mainly needed to dissolve silicates, it seems reasonable to assume that this remaining Fe was sequestered as structural Fe in silicates. This structural Fe can be neglected for estimating the mobility and behavior of Fe (Chen & Ma, 2001; Niskavaara *et al*., 1997). Nevertheless, we reevaluated the Fe isotope compositions of total Fe pool of bulk soil considering the un-extracted Fe in the silicates.

The Fe in silicates has been shown to have positive $\delta^{56}Fe$ values from +0.07 to +1.55‰, in a variety of soil orders from less developed Cambisols to waterlogged Gleysols and to Podzols with characteristic illuvial/eluvial horizons (Wu *et al*., 2019). In the study of Guelke *et al*. (2010), the isotope composition of Fe in silicates were determined in the Ap horizon of a Stagni-Haplic Luvisol after two respective sequential extractions, producing significantly different $\delta^{56}Fe_{Silicate}$ values of +0.41‰ and +0.07‰, respectively. Assuming that the $\delta^{56}Fe_{Silicate}$ values of the un-extracted Fe in our soils were similar to those determined by Guelke *et al*. (2010), we may estimate the theoretical $\delta^{56}Fe$ values of the total Fe pools (Figure S10) with a range from -0.10 to 0.13‰ ($\delta^{56}Fe_{silicate}$ +0.41‰), or from

-0.09 to +0.09‰ ($\delta^{56}Fe_{silicate}$ +0.07‰). These values were identical within analytical uncertainty to the Fe isotope compositions of the Fe pool extracted by our no-HF microwave-assisted digestion. Therefore, the undigested $Fe_{Silicate}$ did not significantly affect the determination of Fe isotope composition of total Fe pool in our soils, showing limited Fe isotope fractionation within a soil profile.

Figures

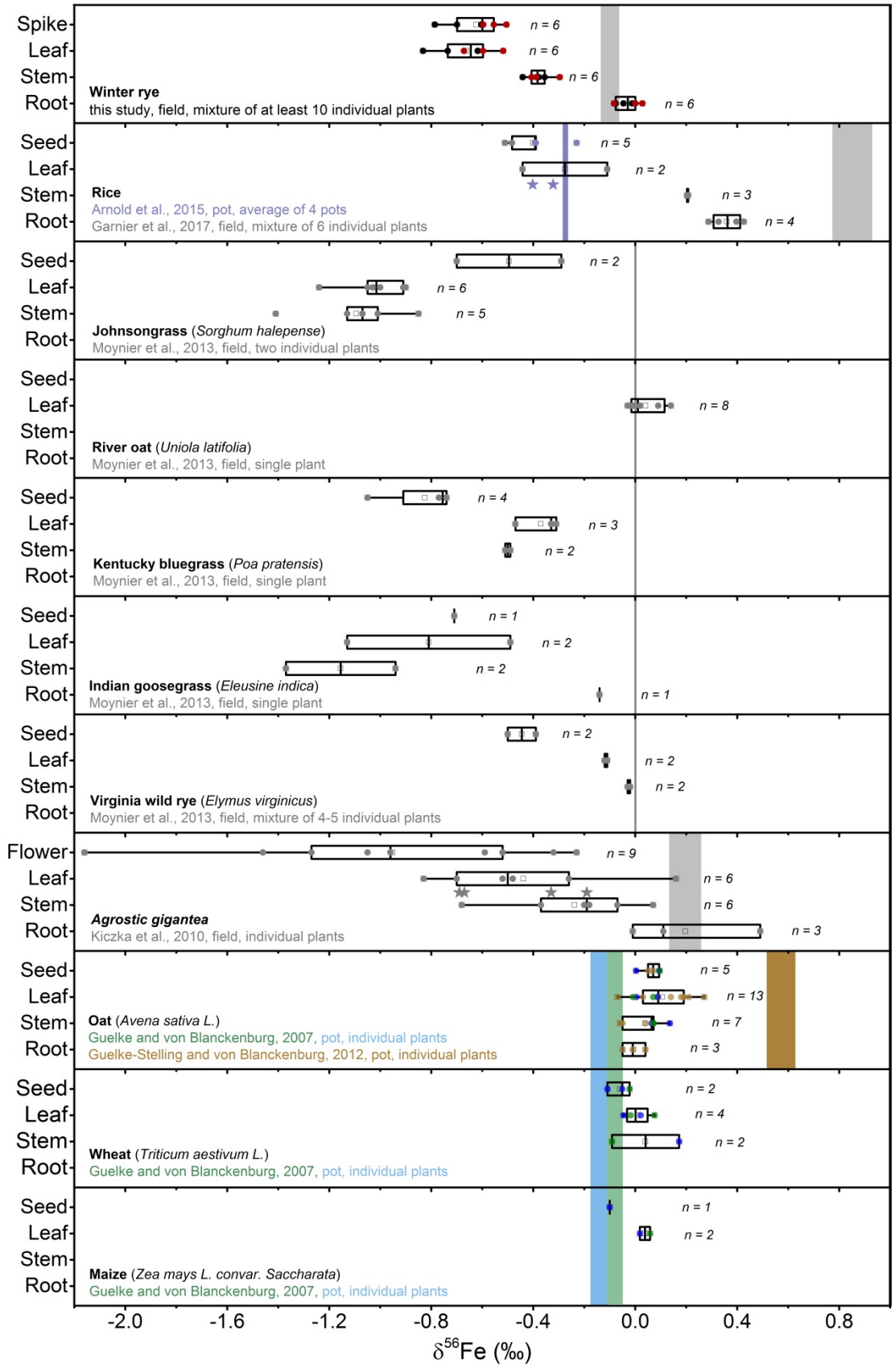
Spike
Leaf
Stem
Root
n = 6
n = 6
n = 6
n = 6
Winter rye
this study, field, mixture of at least 10 individual plants
Seed
Leaf
Stem
Root
n = 5
n = 2
n = 3
n = 4
Rice
Arnold et al., 2015, pot, average of 4 pots
Garnier et al., 2017, field, mixture of 6 individual plants
Seed
Leaf
Stem
Root
n = 2
n = 6
n = 5
Johnsongrass (Sorghum halepense)
Moynier et al., 2013, field, two individual plants
Seed
Leaf
Stem
Root
n = 8
River oat (Uniola latifolia)
Moynier et al., 2013, field, single plant
Seed
Leaf
Stem
Root
n = 4
n = 3
n = 2
Kentucky bluegrass (Poa pratensis)
Moynier et al., 2013, field, single plant
Seed
Leaf
Stem
Root
n = 1
n = 2
n = 2
n = 1
Indian goosegrass (Eleusine indica)
Moynier et al., 2013, field, single plant
Seed
Leaf
Stem
Root
n = 2
n = 2
n = 2
Virginia wild rye (Elymus virginicus)
Moynier et al., 2013, field, mixture of 4-5 individual plants
Flower
Leaf
Stem
Root
n = 9
n = 6
n = 6
n = 3
Agrostic gigantea
Kiczka et al., 2010, field, individual plants
Seed
Leaf
Stem
Root
n = 5
n = 13
n = 7
n = 3
Oat (Avena sativa L.)
Guelke and von Blanckenburg, 2007, pot, individual plants
Guelke-Stelling and von Blanckenburg, 2012, pot, individual plants
Seed
Leaf
Stem
Root
n = 2
n = 4
n = 2
Wheat (Triticum aestivum L.)
Guelke and von Blanckenburg, 2007, pot, individual plants
Seed
Leaf
Stem
Root
n = 1
n = 2
Maize (Zea mays L. convar. Saccharata)
Guelke and von Blanckenburg, 2007, pot, individual plants
-2.0
-1.6
-1.2
-0.8
-0.4
0.0
0.4
0.8
δ56Fe (‰)

938

Figure S1 Iron isotope compositions of the organs of graminaceous plants, which use the complexation strategy (strategy II) for Fe uptake. The vertical lines/bars indicate the Fe isotope compositions of plant-available Fe in the growth media, except for those in Moynier et al (2013) indicating the δ^{56}Fe value of the bulk soil. The colors of the vertical lines/bars correspond to respective data dots. The stars indicate Fe isotope compositions of shoots including stems/straws and leaves which were analyzed as a whole. The black boxplots present to-date available Fe isotopic data for graminaceous plants. Top lane: this study; black: -Lime; red: +Lime.

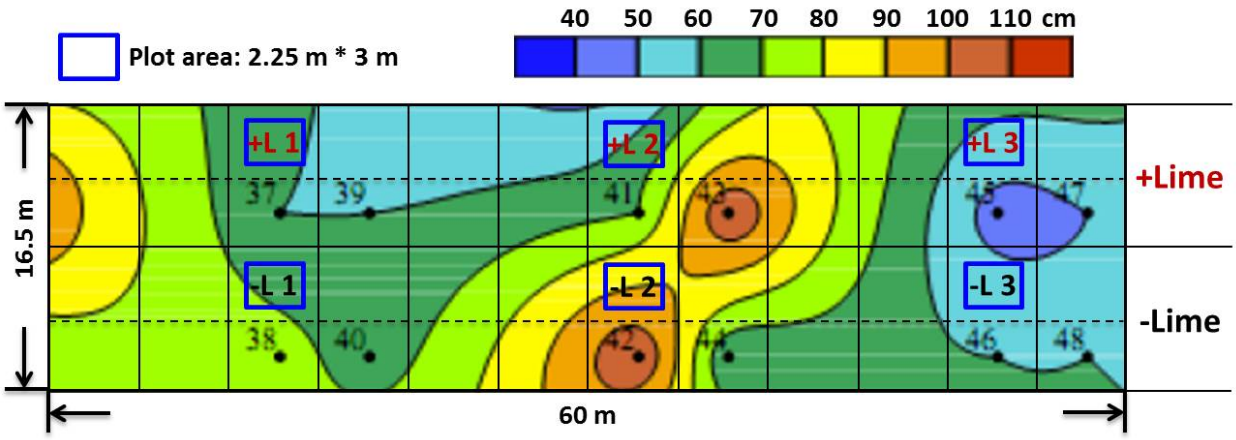

Figure S2 Soil texture change (from sandy to loamy) in the studied filed, showing large heterogeneity mainly in subsoils (modified from Sümer 2012). The blue squares indicate the investigated plots where the soil cores were taken in the present study. The numbers at the background indicate the original sampling points at which the soil texture change was measured (Sümer 2012).

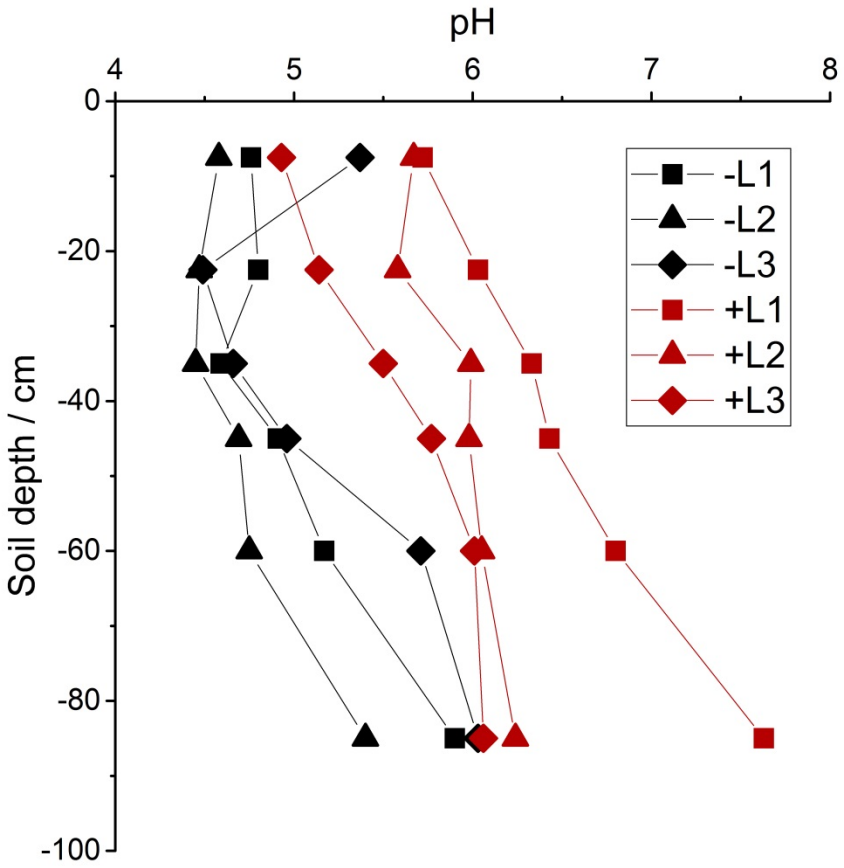

954

955 **Figure SI3** Soil pH values in the investigated plots, showing that the soil pH ($CaCl_2$) was

956 generally about 1 unit higher in the limed plots (+L1, +L2, +L3) than in the non-limed ones

957 (-L1, -L2, -L3).

958

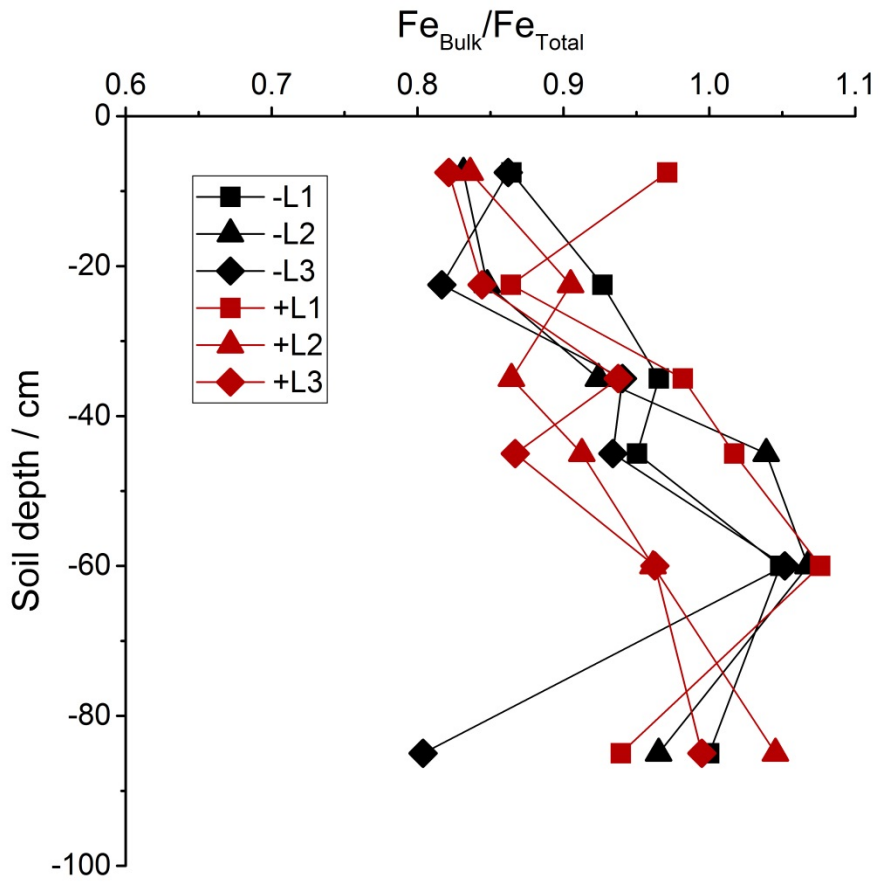

959

960 **Figure S4** The ratio of Fe in bulk soil extracted by pressurized microwave-assisted

961 digestion (Fe_{Bulk}) to that extracted by lithium meta/tetraborate digestion (Fe_{Total}) for soil

962 cores from the limed plots (+L1, +L2, +L3) than in the non-limed ones (-L1, -L2, -L3).

963

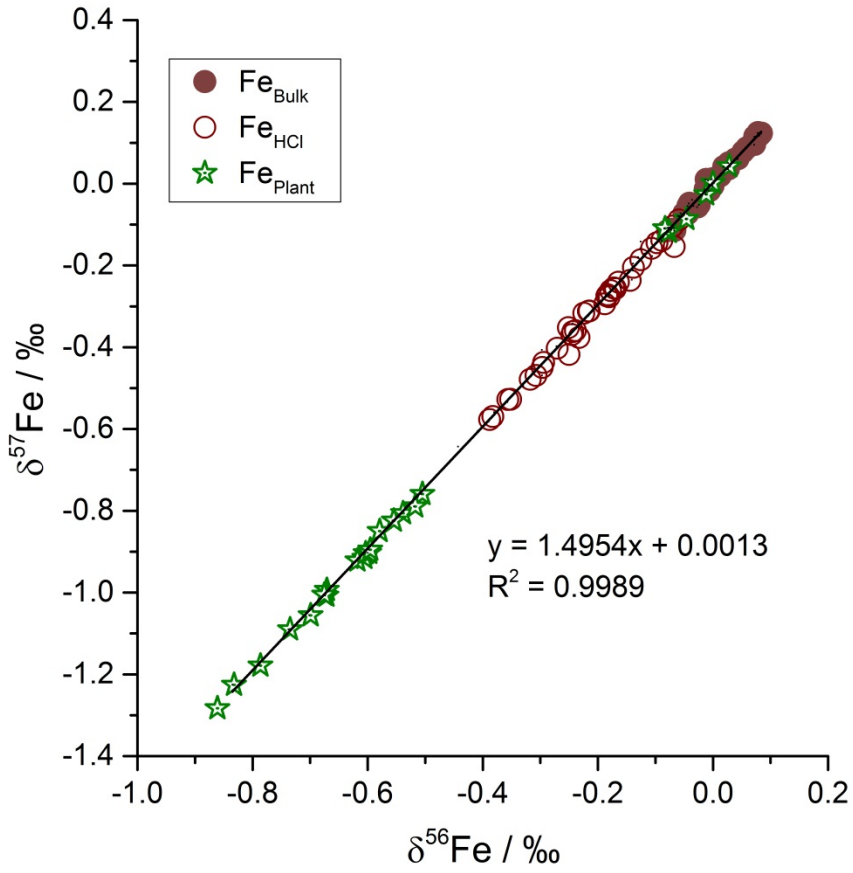

964

965 **Figure S5** Three-isotope-plot displaying measured $\delta^{56}Fe$ and $\delta^{57}Fe$ values of Fe in bulk
966 soil (Fe_{Bulk}, solid brown circle), the HCl-extracted Fe pool (Fe_{HCl}, hollow brown circle), and
967 Fe in plant organs (Fe_{Plant}, green star), the slope (1.4954) of which indicated that Fe
968 isotope fractionation followed the exponential law of mass-dependent fractionation during
969 analyses.

970

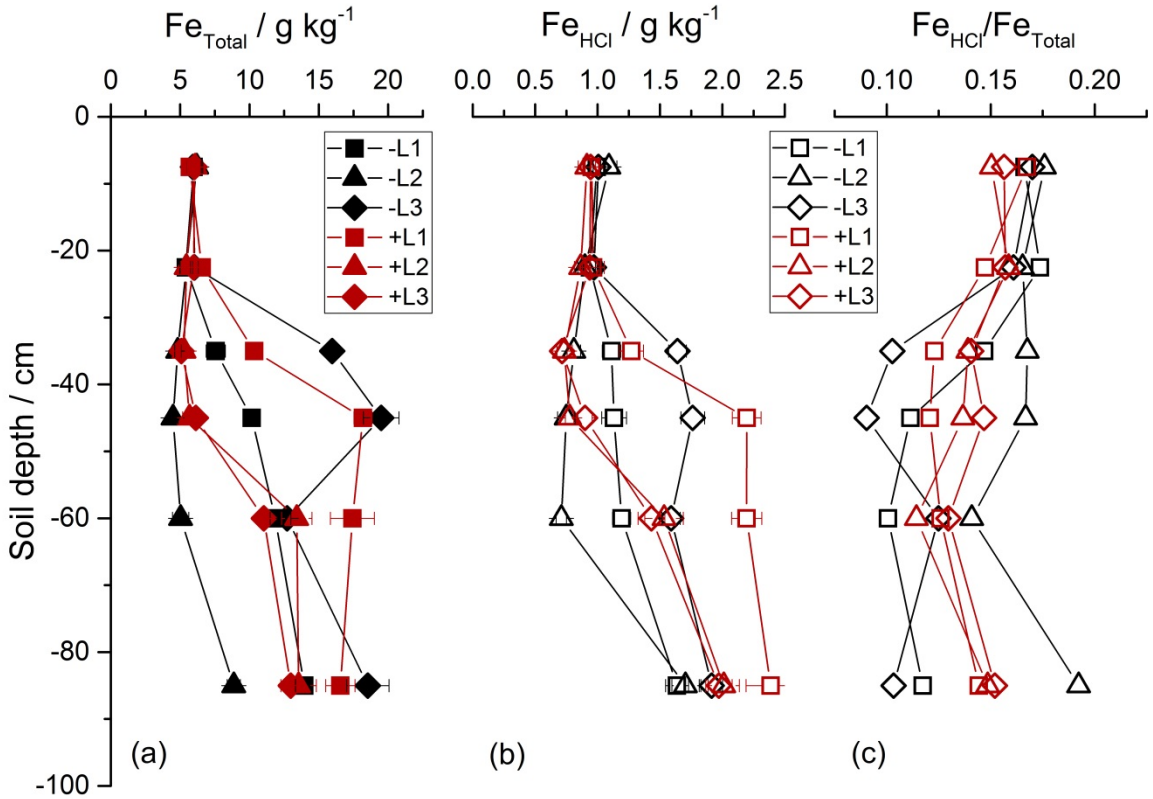

971

972 **Figure S6** Iron concentrations of the total Fe pool (Fe_{Total}) (a) and in the HCl-extractable

973 Fe pool (Fe_{HCl}) (b), and the ratio of Fe_{HCl} to Fe_{Total} (c) in the studied soil profiles.

974

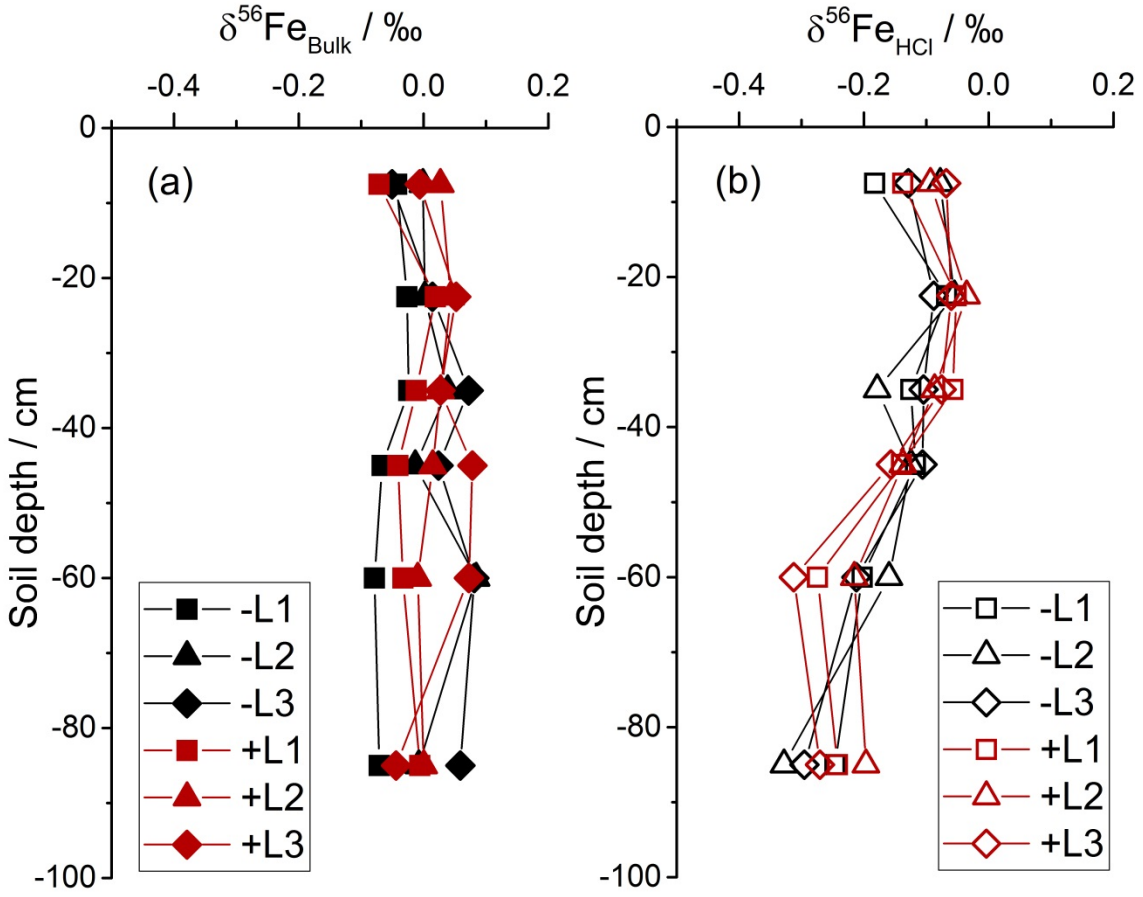

975

976 **Figure S7** Iron isotope compositions of the bulk soil (Fe_{Bulk}) (a) and the Fe_{HCl} pools (b) in
977 each individual plot, showing that the Fe_{HCl} pool, representative of plant-available Fe,
978 exhibited a lighter Fe isotope composition than the bulk soil.

979

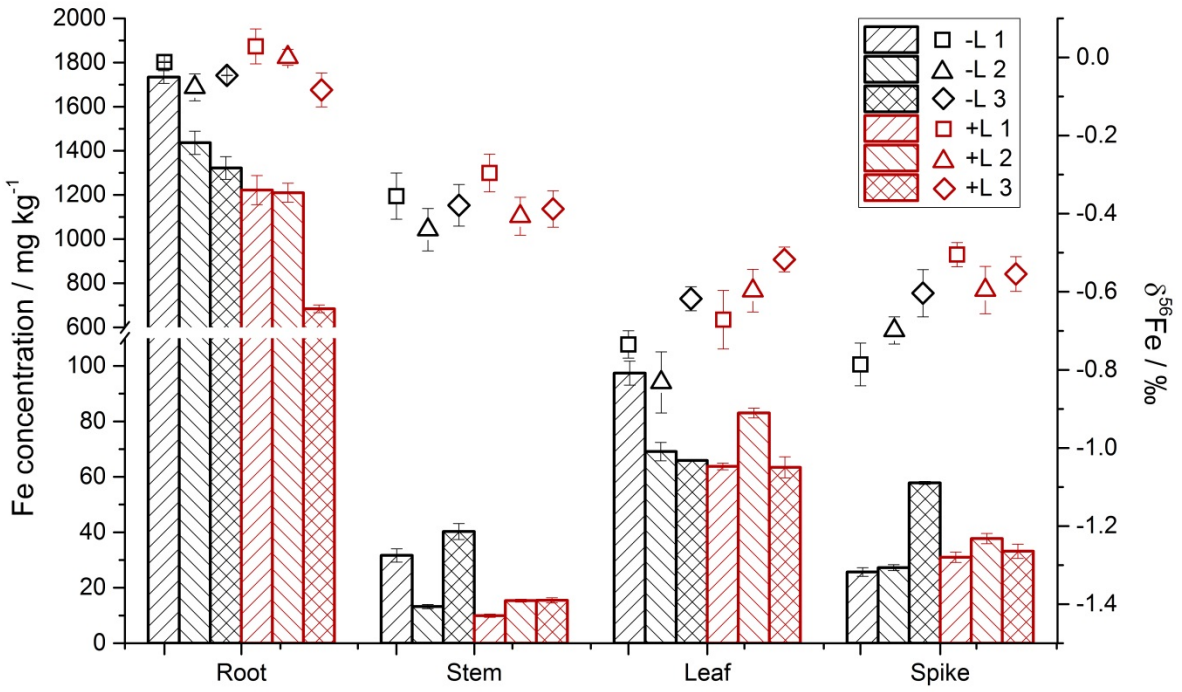

980

981 **Figure S8** Iron concentrations (bars) and Fe isotope compositions (hollow symbols) in
982 various winter rye organs grown in the soils treated with (red) and without (black) lime.
983 The error bars of the concentrations are standard error of the mean of two (root) to six
984 (stem) sample replicates, while the error bars of the δ^{56}Fe values are analytical errors of
985 four measurement replicates.

986

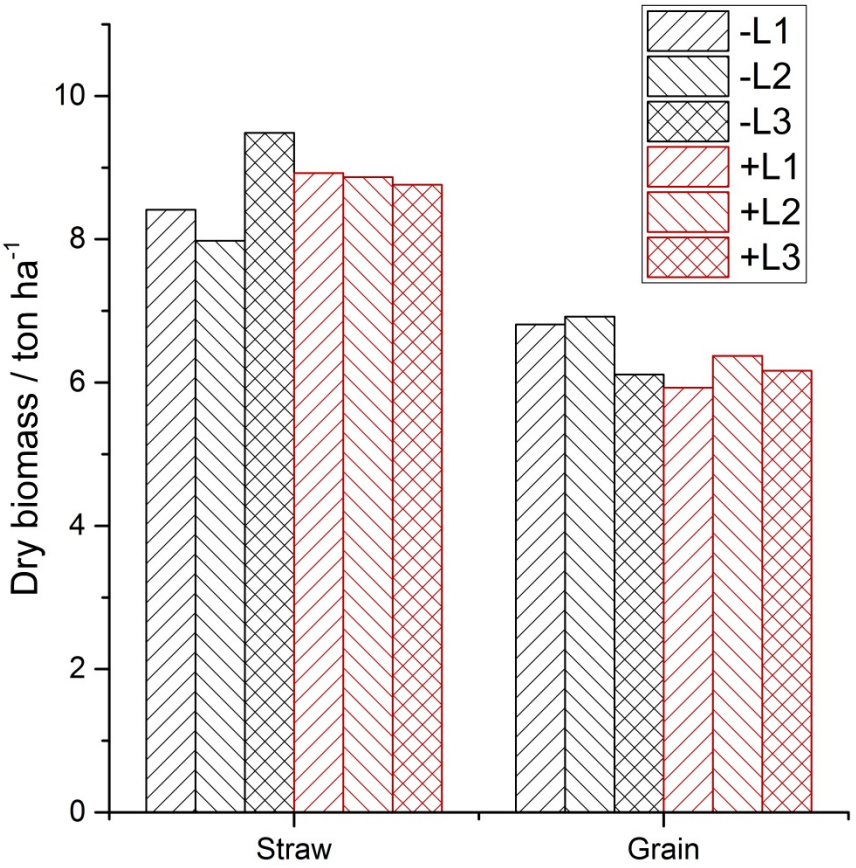

987

988 **Figure S9** Dry biomass of the straw and the grain of winter rye at the harvest in the

989 experimental field in 2017, showing no significant difference in the crop yield between

990 limed and non-limed plots.

991

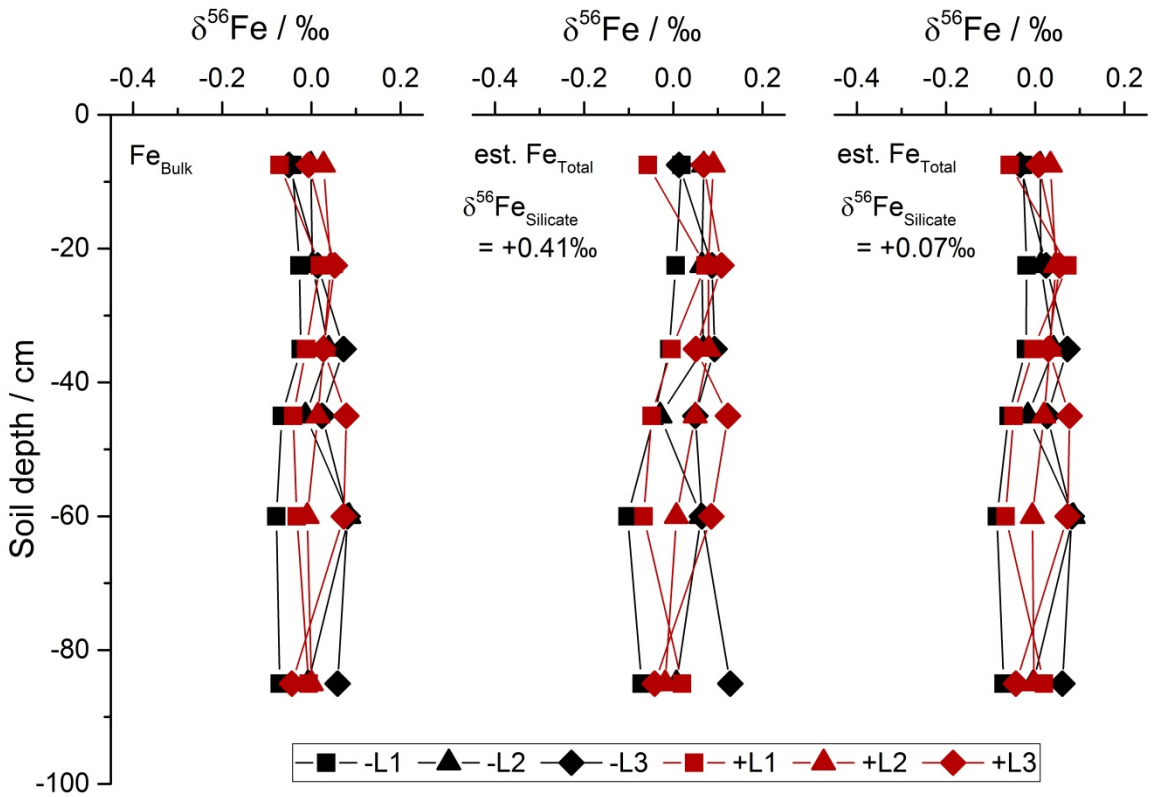

992

993 **Figure S10** Estimated Fe isotope compositions of the total Fe pool in the investigated soil
994 profiles, assuming that the isotope composition of the un-extracted Fe in silicates
995 ($\delta^{56}Fe_{Silicate}$) were +0.41‰ and +0.07‰, as determined on the residues of the two
996 sequential extractions of the A horizon of a Luvisol by Guelker et al. (2010), showing
997 comparable Fe isotope compositions to that of bulk soil extracted by non-HF microwave-
998 assisted digestion (Fe_{Bulk}, left panel).

Tables

Table S1 Iron concentrations and $\delta^{56}Fe$ values of the in-house standard for soils and the NIST SRM 1575a, which were determined together with the soil and plant samples, respectively.

Standard	Fe / mg kg^{-1} [a]		n[b]	$\delta^{56}Fe$ / ‰		n[b]
	mean	SE		mean	SE	
In-house standard for soils	20411	481	6	0.00	0.02	6
(in-lab value)[c]	(20656)	(975)	(48)	(0.01)	(0.01)	(48)
NIST SRM 1575a Pine Needles	44	1	24	-1.43	0.04	6
(in-lab value)[c]	(45)	(3)	(62)	(-1.51)	(0.03)	(14)

[a] Extracted by non-HF pressurized microwave-assisted extraction

[b] the number of measured samples

[c] the values in parentheses are the mean values routinely obtained at IBG-3, FZJ

Table S2 Iron concentrations, stock, and isotope compositions of the total Fe pool and HCl-extractable Fe pool in the studied limed and non-limed plots.

Management	Plot	Soil segment /cm	Soil horizon[a]	Fe_{Total}[c] / g kg^{-1}		Fe_{Bulk}[c] / g kg^{-1}		Fe_{HCl}[c] / g kg^{-1}		Fe_{Total} stock[c] / ton ha^{-1}		Fe_{HCl} stock[c] / ton ha^{-1}		$\delta^{56}Fe_{Bulk}$[d] / ‰		$\delta^{56}Fe_{HCl}$[d] / ‰	
				Mean	SE	Mean	SE	Mean	SE	Mean	SE	Mean	SE	Mean	2SD	Mean	2SD
-Lime +P +FYM deep plough	-L1	0-15	Ap1	6.0	0.4	5.2	0.1	0.99	0.03					-0.04	0.02	-0.18	0.03
		15-30	Ap2	5.4	0.3	5.0	0.1	0.94	0.10					-0.03	0.01	-0.07	0.03
		30-40	Bv-Ael1	7.6	0.5	7.3	0.0	1.11	0.07					-0.02	0.01	-0.12	0.01
		40-50	Bv-Ael2	10.2	0.2	9.7	0.6	1.13	0.10					-0.07	0.04	-0.12	0.04
		50-70	Ael+Bt	11.9	0.3	12.4	0.1	1.19	0.07					-0.08	0.04	-0.20	0.03
		70-100	Bt	14.0	0.4	14.0	1.0	1.64	0.09					-0.07	0.01	-0.25	0.00
		Topsoil (0-30)[b]												-0.03	0.03	-0.12	0.04
		Subsoil (30-100)[b]												-0.07	0.02	-0.21	0.02
		Full profile (0-100)[b]								169	9	21	1	-0.06	0.02	-0.19	0.02
	-L2	0-15	Ap1	6.2	0.4	5.2	0.1	1.09	0.06					0.00	0.03	-0.08	0.05
		15-30	Ap2	5.4	0.5	4.6	0.2	0.90	0.08					0.00	0.02	-0.05	0.04
		30-40	Bv-Ael1	4.8	0.2	4.5	0.2	0.81	0.05					0.04	0.02	-0.18	0.05
		40-50	Bv-Ael2	4.5	0.4	4.7	0.4	0.75	0.07					-0.01	0.02	-0.12	0.04
		50-70	Ael+Bt	5.0	0.6	5.4	0.3	0.71	0.04					0.08	0.03	-0.16	0.02

		70-100	Bt	8.9	0.5	8.6	0.6	1.70	0.11					-0.01	0.02	-0.33	0.04
		Topsoil (0-30)[b]												0.00	0.03	-0.07	0.07
		Subsoil (30-100)[b]												0.02	0.02	-0.27	0.06
		Full profile (0-100)[b]								104	6	19	0	0.01	0.02	-0.22	0.05
	-L3	0-15	Ap1	5.9	0.0	5.1	0.3	1.01	0.04					-0.05	0.04	-0.13	0.03
		15-30	Ap2	6.0	0.3	4.9	0.5	0.97	0.04					0.01	0.05	-0.09	0.03
		30-40	Bv-Ael1	16.0	0.3	15.0	0.7	1.64	0.07					0.07	0.02	-0.10	0.01
		40-50	Bv-Ael2	19.5	1.3	18.2	1.0	1.76	0.09					0.02	0.04	-0.11	0.03
		50-70	Ael+Bt	12.7	0.3	13.4	1.2	1.59	0.07					0.08	0.01	-0.21	0.00
		70-100	Bt	18.5	1.5	14.9	0.4	1.91	0.09					0.06	0.01	-0.30	0.02
		Topsoil (0-30)[b]												-0.02	0.07	-0.11	0.04
		Subsoil (30-100)[b]												0.06	0.02	-0.23	0.03
		Full profile (0-100)[b]								237	4	26	1	0.05	0.02	-0.21	0.02
+Lime	+L1	0-15	Ap1	5.7	0.3	5.5	0.1	0.95	0.05					-0.07	0.03	-0.14	0.04
+P		15-30	Ap2	6.6	0.3	5.7	0.1	0.97	0.09					0.02	0.04	-0.05	0.03
+FYM		30-40	Bv-Ael1	10.3	0.3	10.2	0.0	1.27	0.10					-0.01	0.02	-0.06	0.02
deep plough		40-50	Bv-Ael2	18.2	0.7	18.5	0.6	2.19	0.12					-0.04	0.02	-0.14	0.02
		50-70	Ael+Bt	17.4	1.6	18.7	0.4	2.19	0.12					-0.03	0.02	-0.27	0.02
		70-100	Bt	16.6	1.1	15.5	0.7	2.39	0.20					-0.01	0.02	-0.24	0.01

	Topsoil (0-30)[b]												-0.02	0.06	-0.09	0.05
	Subsoil (30-100)[b]												-0.02	0.02	-0.22	0.02
	Full profile (0-100)[b]								251	16	34	1	-0.02	0.02	-0.12	0.01
+L2	0-15	Ap1	6.1	0.3	5.1	0.4	0.91	0.07					0.03	0.01	-0.09	0.03
	15-30	Ap2	5.5	0.4	4.9	0.2	0.87	0.05					0.04	0.01	-0.04	0.06
	30-40	Bv-Ael1	5.3	0.3	4.6	0.4	0.73	0.06					0.03	0.02	-0.09	0.07
	40-50	Bv-Ael2	5.7	0.5	5.2	0.1	0.78	0.03					0.01	0.03	-0.14	0.03
	50-70	Ael+Bt	13.4	1.1	12.9	0.9	1.53	0.15					-0.01	0.01	-0.22	0.03
	70-100	Bt	13.5	1.3	14.2	1.0	2.01	0.12					0.00	0.02	-0.20	0.04
	Topsoil (0-30)[b]												0.04	0.01	-0.06	0.07
	Subsoil (30-100)[b]												0.00	0.03	-0.18	0.05
	Full profile (0-100)[b]								159	16	25	2	0.01	0.02	-0.12	0.03
+L3	0-15	Ap1	6.0	0.3	5.0	0.3	0.94	0.00					-0.01	0.03	-0.07	0.04
	15-30	Ap2	6.0	0.2	5.0	0.3	0.94	0.01					0.05	0.04	-0.06	0.01
	30-40	Bv-Ael1	5.1	0.3	4.8	0.3	0.72	0.04					0.03	0.04	-0.08	0.01
	40-50	Bv-Ael2	6.1	0.3	5.3	0.4	0.90	0.06					0.08	0.02	-0.16	0.02
	50-70	Ael+Bt	11.0	0.2	10.6	0.7	1.43	0.11					0.07	0.01	-0.31	0.06
	70-100	Bt	13.0	0.1	12.9	1.0	1.97	0.11					-0.04	0.04	-0.27	0.00
	Topsoil (0-30)[b]												0.03	0.05	-0.06	0.04

	Subsoil (30-100)[b]					0.01	0.05	-0.24	0.03
	Full profile (0-100)[b]	148	0	25	2	0.01	0.04	-0.22	0.03

[a] The soil horizons are German descriptions of a representative key soil profile at the experimental site, where Ap is the ploughed topsoil, Bv-Ael and Ael correspond to an eluvial horizon, and Ael+Bt and Bt to an argic horizon according to World Reference Base (IUSS Working Group WRB, 2015).

[b] Rows: calculated $\delta^{56}Fe$ values based on mass balance, see Section 2.4, the error of which (2SD) were propagated error (see Supplementary Information)

[c] Column: data of Fe concentrations and stocks are given as the mean and the standard error of the mean of two sample replicates for each soil core segment. Fe_{Total}: digested by lithium meta/tetraborate digestion, Fe_{Bulk}: digested by pressurized microwave-assisted digestion without HF, Fe_{HCl}: extracted by 0.5 M HCl.

[d] Column: data of Fe isotope compositions are given as the mean and 2SD of four measurement replicates for each sample.

Table S3 Dry biomass, Fe concentrations and isotope compositions of the plant (winter rye) samples.

Management	Plot	Plant organ	Dry biomass[a] / g	Fe[c] / mg kg^{-1}		$\delta^{56}Fe$[d] / ‰		$\Delta^{56}Fe_{Shoot-Root}$[e] / ‰		$\Delta^{56}Fe_{Root-HCl}$[e] / ‰		$\Delta^{56}Fe_{WholePlant-HCl}$[e] / ‰	
				Mean	SE	Mean	2SD	Mean	2SD	Mean	2SD	Mean	2SD
-Lime +P +FYM deep plough	-L1	Root	1.68	1734	50	-0.01	0.00			0.11	0.04		
		Stem	29.85	32	4	-0.36	0.06						
		Leaf	6.33	97	7	-0.73	0.03						
		Spike	1.30	26	3	-0.79	0.05						
		Shoot[b]				-0.51	0.10	-0.50	0.10				
		Whole plant[b]				-0.19	0.06					-0.07	0.08
	-L2	Root	2.20	1436	91	-0.08	0.03			-0.01	0.10		
		Stem	29.13	13	1	-0.44	0.05						
		Leaf	9.14	69	6	-0.83	0.08						
		Spike	2.63	27	2	-0.70	0.03						
		Shoot[b]				-0.68	0.14	-0.61	0.15				
		Whole plant[b]				-0.23	0.09					-0.17	0.09
	-L3	Root	2.52	1322	89	-0.05	0.00			0.06	0.04		
		Stem	33.30	40	5	-0.38	0.05						

		Leaf	8.70	66	0	-0.62	0.03						
		Spike	2.28	58	1	-0.60	0.06						
		Shoot[b]				-0.46	0.10	-0.41	0.10				
		Whole plant[b]				-0.20	0.06					-0.10	0.06
+Lime	+L1	Root	3.13	1222	115	0.03	0.04			0.12	0.10		
+P		Stem	29.51	10	1	-0.30	0.05						
+FYM		Leaf	9.82	64	2	-0.67	0.07						
deep plough		Spike	3.92	31	3	-0.50	0.03						
		Shoot[b]				-0.55	0.13	-0.57	0.16				
		Whole plant[b]				-0.09	0.10					0.00	0.11
	+L2	Root	5.73	1210	74	0.00	0.02			0.07	0.08		
		Stem	25.36	15	1	-0.41	0.05						
		Leaf	9.37	83	3	-0.60	0.05						
		Spike	3.21	38	3	-0.60	0.06						
		Shoot[b]				-0.54	0.11	-0.54	0.11				
		Whole plant[b]				-0.08	0.06					-0.02	0.06
	+L3	Root	5.77	684	30	-0.08	0.04			-0.02	0.09		
		Stem	33.38	15	2	-0.39	0.05						

Leaf	9.04	63	7	-0.52	0.03				
Spike	6.72	33	4	-0.55	0.04				
Shoot[b]				-0.47	0.08	-0.39	0.12		
Whole plant[b]				-0.18	0.09			-0.12	0.09

[a] Pooled plant samples, which were weighed after separation of organs and drying. After weighting the plant samples were milled, the subsamples of which were used for Fe concentration and isotope composition analyses.

[b] Row: Calculated $\delta^{56}Fe$ values based on mass balance, see Section 2.4, the error of which (2SD) were propagated error (see Supplementary Information)

[c] Column: data of Fe concentrations and stocks are given as the mean and the standard error of the mean of two (root) to six (spike) sample replicates for each plant organ.

[d] Column: data of Fe isotope compositions are given as the mean and the two standard deviation of four measurement replicates for each sample.

[e] Column: apparent difference in Fe isotope compositions between Fe pool A and B, see Section 2.4, the error of which (2SD) were propagated error (see Supplementary Information). Note that $\delta^{56}Fe_{HCl}$ in topsoil was used for comparison with those in plants.

Reference

Ad-hoc-AG Boden (2005). Bodenkundliche Kartieranleitung (5th ed.). Bundesanstalt für Geowissenschaften und Rohstoffe und Staatlichen Geologischen Diensten der Bundesländer der Bundesrepublik Deutschland. (Ad-hoc-AG Soil (2005). Soil science mapping instructions (5th ed.). Federal Institute for Geosciences and Natural Resources and State Geological Services of the Länder of the Federal Republic of Germany.)

Arnold, T., Markovic, T., Kirk, G.J.D., Schönbächler, M., Rehkämper, M., Zhao, F.J. & Weiss, D.J. (2015). Iron and zinc isotope fractionation during uptake and translocation in rice (*Oryza sativa*) grown in oxic and anoxic soils. Comptes Rendus Geoscience, 347, 397-404. doi:10.1016/j.crte.2015.05.005

Bauke, S. L., von Sperber, C., Tamburini, F., Gocke, M. I., Honermeier, B., Schweitzer, K., Baumecker, M., Don, A., Sandhage-Hofmann, A. & Amelung, W. (2018). Subsoil phosphorus is affected by fertilization regime in long-term agricultural experimental trials. European Journal of Soil Science, 69, 103-112. doi:10.1111/ejss.12516

Chen, M. & Ma, L. Q. (2001). Comparison of three aqua regia digestion methods for twenty florida soils. Soil Science Society of America Journal, 65, 491-499. doi:10.2136/sssaj2001.652491x

Dauphas, N., Janney, P. E., Mendybaev, R. A., Wadhwa, M., Richter, F. M., Davis, A. M., van Zuilen, M., Hines, R. & Foley, C. N. (2004). Chromatographic separation and multicollection-ICPMS analysis of iron. Investigating mass-dependent and –independent isotope effects. Analytical Chemistry, 76, 5855-5863. doi:10.1021/ac0497095

Dauphas, N., John, S. & Rouxel, O. (2017). Iron isotope systematics. Reviews in Mineralogy and Geochemistry, 82, 415-510. doi:10.2138/rmg.2017.82.11

Garnier, J., Garnier, J.-M., Vieira, C.L., Akerman A., Chmeleff, J., Ruiz, R.I. & Poitrasson F. (2017). Iron isotope fingerprints of redox and biogeochemical cycling in the soil-water-rice plant system of a paddy field, Science of Total Environment, 574, 1622–1632. doi:10.1016/j.scitotenv.2016.08.202

Guelke, M. & von Blanckenburg, F. (2007). Fractionation of stable iron isotopes in higher plants. Environment Science and Technology, 41, 1896-1901. doi:10.1021/es062288j

Guelke, M., von Blanckenburg, F., Schoenberg, R., Staubwasser, M. & Stuetzel H. (2010). Determining the stable Fe isotopic signature of plant-available iron in soils. Chemical Geology, 277, 269–280. doi:10.1016/j.chemgeo.2010.08.010

Guelke-Stelling, M. & von Blanckenburg, F. (2012). Fe isotope fractionation caused by translocation of iron during growth of bean and oat as models of strategy I and II plants. Plant and Soil, 352, 217–231. doi:10.1007/s11104-011-0990-9

Hobley, E. U., Honermeier, B., Don, A., Gocke, M. I., Amelung, W. & Kögel-Knabner, I. (2018). Decoupling of subsoil carbon and nitrogen dynamics after long-term crop rotation and fertilization. Agriculture, Ecosystems & Environment, 265, 363-373. doi:10.1016/j.agee.2018.06.021

Kiczka, M., Wiederhold, J. G., Kraemer, S. M., Bourdon, B. & Kretzschmar, R. (2010). Iron isotope fractionation during plant uptake and translocation in alpine plants. Environmental Science & Technology, 44, 6144–6150. doi:10.1021/es100863b

Köhn, W. & Ellmer, F. (2009). Dauerfeldversuche in Brandenburg und Berlin. Beiträge für eine nachhaltige Landwirtschaftliche Bodennutzung (Long-term field tests in Brandenburg and Berlin. Contributions to sustainable agricultural land use). State

Office for Consumer Protection, Agriculture and Land Consolidation, Department of Agriculture and Horticulture, Series in Agriculture, 10, 216.

IUSS Working Group WRB. (2015). World Reference Base for Soil Resources 2014, Update 2015, International Soil Classification System for Naming Soils. World Soil Resources Report 106. Food and Agriculture Organization of the United Nations, Rome.

Moynier, F., Fujii, T., Wang, K. & Foriel, J. (2013). Ab initio calculations of the Fe (II) and Fe (III) isotopic effects in citrates, nicotianamine, and phytosiderophore, and new Fe isotopic measurements in higher plants. Comptes Rendus Geoscience, 345, 230-240. doi:10.1016/j.crte.2013.05.003

Niskavaara, H., Reimann, C., Chekushin, V. & Kashulina, G. (1997). Seasonal variability of total and easily leachable element contents in topsoils (0–5 cm) from eight catchments in the European arctic (Finland, Norway, and Russia). Environmental Pollution, 96, 261–274. doi:10.1016/S0269-7491(97)00031-6

OriginLab. (2015). OriginPro. Release b9.2.272., OriginLab, Northampton, MA.

Sarkar, A.N. & Wynjones, R.G. (1982). Effect of rhizosphere pH on the availability and uptake of Fe, Mn and Zn. Plant and Soil, 66, 361–372. doi:10.1007/BF02183802

Schwartz, V. & Kölbel, M. (1992). Vergleich verschiedener Aufschluß methoden zur quantitativen Erfassung der Elementgesamtgehalte in Abhängigkeit von der Bodenausbildung (Comparison of different digestion methods for the quantitative determination of the total element contents depending on the soil formation). Z. Pflanzenernähr. Bodenkd. (Journal of Plant Nutrition and Soil Science), 155, 281-284. doi:10.1002/jpln.19921550407

Sümer, M. R. (2012). Auswirkungen verschiedener Bodennutzungssysteme auf ausgewählte physiko-chemische Bodeneigenschaften und pflanzenbauliche

Parameter in Berlin-Dahlem und Dedelow (Effects of different land use systems on selected physicochemical soil properties and plant-growing parameters in Berlin-Dahlem and Dedelow). Doctoral dissertation, Humboldt-Universität zu Berlin, Berlin.

Walter, K., Don, A., Tiemeyer, B. & Freibauer, A. (2016). Determining soil bulk density for carbon stock calculation: a systematic method comparison. Soil Science Society of America Journal, 80, 579–591. doi:10.2136/sssaj2015.11.0407